

SENSE AND PURIFY: DETECT, DESTROY AND REMOVE WATER CONTAMINANTS (SPY)

Report to the
Water Research Commission

by

Kefilwe V. Mokwebo, Samantha F. Douman and Emmanuel I. Iwuoha
Department of Chemistry, University of the Western Cape

WRC Report No. 3024/1/22
ISBN 978-0-6392-0183-2

July 2022



Obtainable from

Water Research Commission
Private Bag X03
Gezina
PRETORIA, 0031

orders@wrc.org.za or download from www.wrc.org.za

This is the final report of WRC project no. C2019/20-0008.

DISCLAIMER

This report has been reviewed by the Water Research Commission (WRC) and approved for publication. Approval does not signify that the contents necessarily reflect the views and policies of the WRC, nor does mention of trade names or commercial products constitute endorsement or recommendation for use.

EXECUTIVE SUMMARY

BACKGROUND

One of the programmes of the European Union Horizon 2020 ERA-Net Cofund Action Water Works 2017 Joint Programming Initiative is the “Water Challenges for a Changing World (Water JPI). Sense and Purify (SPy) was one of the research projects approved under the Water JPI 2018 Joint Call for Closing the Water Cycle Gap – Improving Sustainable Water Resource Management. Generally, the research projects of the Water JPI 2018 Joint Call involved the development of innovative technological protocols for bridging the supply and demand gap through sustainable water resources management. The SPy project aimed at developing sustainable and cost-effective integrated electrochemical technologies for the detection, measurement and elimination of active pharmaceutical ingredients (APIs) from urban wastewater to make it suitably usable. The SPy project involved a consortium consisting of Dublin City University (DCU) (Ireland), University of Nantes (France), Universitat Rovira i Virgili (URV) (Spain) and the University of the Western Cape (UWC) (South Africa). The Water Research Commission (WRC) was the co-fund partner for South Africa. The UWC team focussed its studies on antiretroviral (ARV) drugs (or antiretrovirals, ARVs) which were the types of APIs considered to be prevalent in South Africa.

The high rate of production and consumption of ARVs for the prevention and treatment of human immunodeficiency virus (HIV) in South Africa has resulted in their contamination of, and persistence in, aquatic environment. ARV drugs consumed by HIV patients are only partially metabolised and are excreted as APIs into the domestic and hospital wastewater sewage systems. Since many ARVs are resistant to biodegradation in activated sludge, they remain in the wastewater effluent and are continuously discharged into nearby water sources. This results in their environmental accumulation and potentially adverse effects on aquatic biota and terrestrial lives that inhabit and/or consume the contaminated water. Moreover, their long-term presence in the environment may be harmful to human through the creation of resistant viruses and bacteria.

Although South Africa has the highest consumption rate of ARV drugs in the world, it does not have extensive environmental programs and legislation regarding the maximum permissible concentration of ARVs in the environment. Therefore, there is a need for routine monitoring of the level of these micropollutants in the aquatic environment in order to minimize their effect on aquatic biota. To perform the task, accurate, reliable, sensitive, and robust analytical tools that will monitor the quantity of these emerging micropollutants are required. Liquid chromatography coupled with mass spectrometry hyphenated techniques has been successful and effective in monitoring a wide range of pharmaceuticals (including ARVs) in complex environmental samples at the trace level. However, there are some drawbacks associated with them. On the other hand, electroanalysis (using electrochemical sensors) is a very promising and efficient alternative for monitoring ARVs onsite at a low cost compared to chromatographic techniques. Due to their high prescription rate and frequent detection at higher concentrations in South African wastewater and surface waters, nevirapine (NVP), tenofovir (TNF), and emtricitabine (FTC) were chosen for this study. The present study explores the electrochemical kinetics of the selected ARV and also their electroanalysis in wastewater treatment plant effluent and tap/drinking water.

AIMS

The following were the aims of the overall SPY project to which the DCU, UN, URV and UWC teams were to contribute:

1. Development of sensors for wastewater. (The UWC part of the consortium will develop highly sensitive and cost-effective sensor reactors for recalcitrant organics such as antibiotics and other APIs in industrial and domestic wastewaters.)
2. Wireless bipolar electrochemistry-based reactor for wastewater treatment.
3. High performance electrochemiluminescent (ECL) sensors.

4. ECL immunosensors and aptasensors (Pharmaceutical organic contaminants will be detected and mineralised using electrochemically charged BDD particles in the wireless ECL reactor-based Spy technology.)
5. The communication of the technology to interest groups, stakeholders and policy makers.

METHODOLOGY

The contribution of the UWC team to project is divided into three. The first two studies focused on the development, characterization and optimization of a boron-doped diamond electrochemical reactor (BDD reactor) for the sensing and the mineralisation (i.e. the elimination) of nevirapine (NVP) and tenofovir (TNF) in wastewater samples. Cyclic voltammetry (CV) and square wave (SWV) were used to investigate the amperometric response and electro-oxidation characteristics of NVP and TNF at the BDD reactor at various pH values. It was also necessary to study the electro-oxidation kinetics of the drugs at the BDD reactor. The determination of NVP and TNF in wastewater and tap water was carried out using differential pulse voltammetry (DPV). More details on the methods employed for the electroanalysis of NVP and TNF are presented in Chapter 3.

The third study involved the determination of emtricitabine (FTC) using a magnetically active molecularly imprinted polymer (MIP) electrochemical reactor as the sensor. The working electrode was a glassy carbon electrode (GCE) which was modified with iron oxide nanoparticles (Fe_3O_4) and para-aminobenzoic acid (PABA)-based MIP to increase the sensitivity and the selectivity of the sensor for FTC. The MIP technology involves the imprinting of the emtricitabine as a molecular template on the poly(para-aminobenzoic acid) polymer matrix. The imprinted FTC template is then removed or eluted from the polymer matrix using a suitable solvent (methanol: acetic acid). The sensor detection processes involves the binding of the FTC on the structurally specific cavity created on the polymer, which then produces a measurable signal. Detailed information on this method is also presented in Chapter 3.

The limit of detection (LOD) and the limit of quantification (LOQ) for all the sensors were determined using the slope of the calibration curve, the standard deviation of the blank ($n = 6$) and signal to noise ratio values of 3.3 for LOD and 10 for LOQ.

RESULTS AND DISCUSSIONS

This study explored the use of voltammetric methods for electroanalysis of antiretroviral drugs in the environment. Voltammetry was chosen because it can provide both qualitative and quantitative information about the analyte of interest. For successful electrochemical sensing and mineralization of these micropollutants in wastewater, one needs to understand their electrochemical nature when they are stimulated by an electrical parameter (e.g. potential). Moreover, the electrode material and surface also affect the electrochemistry of the developed method. CV and SWV were used to investigate the influence of pH on the position, intensity, and morphology of both NVP and TNF electrochemical signals at the BDD reactor. NVP electroanalysis was carried out on a cathodically pretreated BDD electrode. Cathodically pretreating the BDD resulted in a hydrogen-terminated (H^+) hydrophobic electrode surface. The positive charges on the electrode surface attracted the negatively charged NVP forming hydrogen bonds which facilitated electrode electron transfer between the analyte and the electrode surface. An anodically pretreated BDD produced poor signals of NVP, as the charges were repelling each other. For TNF electroanalysis, an anodically pretreated BDD reactor was used (APT-BDD). Anodically pretreating the reactor resulted in oxygen-terminated (O) hydrophilic surface. This surface contained carbonyl and hydroxyl groups that bonded with the positively charged nitrogen of the TNF molecule, resulting in increased electron transfer at the electrode surface. As part of the analysis for direct current (DC) voltammetry results, the following reactor's parameters for the ARV were evaluated; onset potential for sensing (OPS), onset potential for mineralization (OPM) peak potential (E_p), magnitude of sensing signal (MSS) and magnitude of mineralization and oxidation (MOM).

The CV of CPT-BDD in the presence of NVP exhibits one well-defined irreversibly oxidation peak at 0.67 V vs Ag/AgCl. This peak and its electrochemical parameters are affected by the pH. The OPS and OPM and E_p shifts negatively with increasing pH, while MSS and MOM increase. NVP can only be oxidized at neutral and alkaline conditions as there was no oxidation peak observed at pH 2-6. In slightly basic conditions, no protons are involved in the electrooxidation of NVP, and at pH 10-12, the drug loses two electrons, while also gaining two protons. For quantitative studies, the NVP peak current at 0.67 V vs Ag/AgCl increase with increasing concentration from 0.1-50 $\mu\text{g.Ml}^{-1}$ with good linearity of $R^2 = 0.99609$. The developed method had a LOD and LOQ of 0.0368 and 0.123 $\mu\text{g.Ml}^{-1}$, respectively. The sensitivity of the sensor was 11.87 $\mu\text{A}/\mu\text{g.Ml}^{-1}/\text{cm}^2$ with an excellent relative standard deviation (RSD) of 3.58%. The practical applicability of the developed method was tested in wastewater effluent and tap water. For wastewater analysis, NVP recovery varied from 96 ± 4.4 to $101 \pm 0.76\%$, while the recovery in the tap/drinking water ranged from 94 ± 3.2 to $99.4 \pm 0.2\%$. The high recoveries without sample pretreatment confirm that the proposed analytical method can be used for accurate and selective analysis of ARV in complex matrices such as wastewater, biological samples, and pharmaceutical formulations

The CV of TNF also exhibits one well-defined irreversible oxidation peak at 1.42 V vs Ag/AgCl. The oxidation peak is more prominent in acidic media. This peak was due to the electro-oxidation of the pyrimidine base in the adenine base at acid media. The OPS and OPM and E_p shifts negatively with increasing pH. However, at pH 5 and above, the E_p shifting is not much. This is because from pH 2-4, electrooxidation of TNF involves an equal number of protons and electrons, whereas at pH 5-8, the number of protons is half the number of electrons. The MSS and MOM also increase from pH 2-4, and then gradually decrease from pH 5-8. This shows that's the best results to obtain for TNF sensing and mineralization are in an acidic medium. At pH 4, the irreversible oxidation peak current TNF increased with increasing concentration over a wide range of 0.014-7.18 $\mu\text{g.Ml}^{-1}$. The LOD and LOQ for TNF analysis were calculated as 0.00123 and 0.00422 respectively, while sensitivity was 35.56 $\mu\text{A}/\mu\text{g.Ml}^{-1}/\text{cm}^2$. To validate the accuracy of the electrochemical method as well as its practicality, recovery experiments on wastewater and tap water spiked with different concentrations of TNF were performed. The proposed analytical method yielded a recovery ranging from 96.6 ± 3.2 to $99.3 \pm 4.0\%$ LOD of 0.0106 $\mu\text{g.Ml}^{-1}$, and LOQ of 0.0356 $\mu\text{g.Ml}^{-1}$ for wastewater effluent spiked with 0.029, 0.144, 0.289 $\mu\text{g.Ml}^{-1}$ TNF. Tap/drinking water spiked with 0.01, 0.05, and 0.1 $\mu\text{g.Ml}^{-1}$ TNF yielded a recovery percentage ranging from 95 ± 2.7 to $97.8 \pm 3.1\%$ with LOD and LOQ of 0.0159 and 0.0561 $\mu\text{g.Ml}^{-1}$, respectively.

For FTC analysis, a magnetic molecularly imprinted polymer (MMIP) electrochemical sensor was developed. The mechanism used in this study was that, as FTC selectively binds to the cavities created on the imprinted polymer sensor, the peak current of the electroactive polymer will decrease and the peak potential will shift positively because FTC was not electroactive in the potential window (-0.3 to 1.3 V vs Ag/AgCl) that was used for the electrosynthesis of the polymer. FTC is electroactive at very high potential (1.65 V vs Ag/AgCl) and this is usually not favourable, especially when using a glassy carbon electrode which fouls at higher potential. The MMIP provided excellent selectivity and sensitivity towards the detection of FTC as compared to magnetic non-imprinted polymer sensor (MNIP). The use of Fe_3O_4 NPs increased the active surface area of the electrode allowing more FTC molecules to bind on the polymer cavities on the electrode. During optimization studies for MIP preparation, a molar concentration (Mm) of 5:1 for PABA:FTC was used in H_2SO_4 as the electrolyte. The template was eluted from the polymer matrix by immersing the electrode in the stirred eluting solvent (methanol: acetic acid) for 5 min.

The rebinding of the template to the cavities on the polymer took 3 min. After optimization and the template extraction from the MMIP, the fabricated MIP/PABA- Fe_3O_4 /GCE sensor was used for the detection of FTC by immersing the sensor in an electrolyte solution containing different concentrations of FTC for 3 min for the rebinding of the drug on the cavities on the sensor. The current response of the extracted MMIP at 0.51 V gradually decreases with the sequential addition of FTC (0.01 to 100 $\mu\text{g.Ml}^{-1}$), and the peak potential experiences a positive shift with increasing FTC concentration. This was due to the blockage of electron transfer between the polymer and the electrode caused by the non-electroactive FTC on the cavities of the polymer matrix. The developed voltammetric sensor had two linear dynamic ranges at 0.01 to 10 $\mu\text{g.Ml}^{-1}$ and

1.0 to 100 $\mu\text{g}\cdot\text{Ml}^{-1}$. A LOD and LOQ of 0.006 $\mu\text{g}\cdot\text{Ml}^{-1}$ and 0.02 $\mu\text{g}\cdot\text{Ml}^{-1}$ were obtained at a 0.01 to 10 $\mu\text{g}\cdot\text{Ml}^{-1}$ linear concentration range. The use of the sensor in the presence of interferents was also tested, but the sensor demonstrated excellent selectivity to the FTC molecule. This method was not yet tested for its practical application in real wastewater and surface water sample.

CONCLUSION AND RECOMMENDATIONS

In this project, simple and sensitive electroanalytical methods were developed for qualitative and quantitative analysis of NVP, TNF, and FTC in wastewater and tap/drinking water. For electroanalysis, choosing the appropriate electrochemical method and electrode material plays a very important role in enhancing the performance of the method. Usually, voltammetric methods are excellent for electroactive analytes. For non-electroactive analytes, a redox probe is required. BDD is an excellent electrode to perform electroanalysis of organic molecules that are either oxidized or reduced at very high potentials due to its wide potential window and antifouling properties. Therefore it is worth exploring the BDD reactor for electroanalysis of FTC. Moreover, to improve the analytical performance of the analytical method and the BDD reactor, the use of nanomaterials and conducting polymers as electrocatalytic modifiers are recommended. The authors recommend studying the effects of interferents on the developed methods for NVP and TNF analysis. This will assist in also developing a voltammetric method for simultaneous analysis of these drugs as they are usually prescribed in combination. In addition, the electroanalysis of ARV in wastewater, surface water, groundwater, and drinking water should be extensively studied as there are no studies on the environmental electroanalysis of ARV.

South Africa has poor and malfunctioning sewage systems and wastewater treatment plants. Therefore, there is a need for upgrading the existing treatment plants, fixing sewage pipes, and building new wastewater treatment plants to assist the overburdened ones. Moreover, since it has been proven that pharmaceuticals and their residues are reluctant against conventional wastewater treatment technologies, it is worth exploring other technologies such as advanced oxidation processes, membranes, and powdered activated carbon.

Since South Africa does not have enough advanced analytical facilities, instruments, and funding, it is very difficult to carry out research on the presence, toxicity, quantification, and removal of these micropollutants in the environment. Therefore, collaboration or partnership between public and private institutes locally and internationally is required. The partnership will assist in developing extensive environmental monitoring programs and legislation guidelines for ARV waste. We need to determine the permissible level of ARV on the environment so that we can mitigate their effect on the aquatic environment

ACKNOWLEDGEMENTS

The project team wishes to thank the following people for their contributions to the project.

Name	Affiliation
Prof Robert Forster	Dublin City University, Ireland
Prof Ciara O'Sullivan	Universitat Rovira i Virgili, Spain
Prof Yann Pellegrin	University of Nantes, France

This page was intentionally left blank

CONTENTS

EXECUTIVE SUMMARY	iii
ACKNOWLEDGEMENTS	vii
CONTENTS	ix
LIST OF FIGURES	xi
LIST OF TABLES	xii
ACRONYMS & ABBREVIATIONS	xiii
CHAPTER 1: BACKGROUND	1
1.1 INTRODUCTION	1
1.2 AIMS	2
1.3 OBJECTIVES.....	2
1.4 SCOPE AND LIMITATIONS	3
CHAPTER 2: LITERATURE REVIEW	4
2.1 INTRODUCTION	4
2.2 HIV/AIDS AND ANTIRETROVIRAL DRUGS IN SOUTH AFRICA.....	4
2.3 ANTIRETROVIRAL DRUGS IN WASTEWATER AND AQUATIC ENVIRONMENT.....	5
2.3.1 The fate of antiretroviral drugs in wastewater	5
2.3.2 Occurrence of antiretroviral drugs in wastewater	6
2.4 ELECTROANALYSIS AND ELECTROCHEMICAL SENSORS	8
CHAPTER 3: MATERIALS AND METHODS	10
3.1 INTRODUCTION	10
3.2 CHEMICALS AND REAGENTS	10
3.3 INSTRUMENTATION	11
3.4 ELECTROCHEMICAL PROCEDURE	11
3.4.1 Preparation of the BDD working electrode	11
3.4.2 Electrochemical synthesis of magnetic molecularly imprinted polymer (MMIP) and non-imprinted polymer (MNIP) for FTC determination.....	11
3.5 PREPARATION OF WATER SAMPLES	12
CHAPTER 4: RESULTS AND DISCUSSIONS	13
4.1 INTRODUCTION	13
4.2 ELECTRO-OXIDATION AND ANALYSIS OF NVP DRUG ON A BDD REACTOR.....	13
4.2.1 Electrochemical dynamics of NVP at the BDD reactor	13
4.2.2 Effect of pH on electro-oxidation parameters of NVP at the BDD reactor.....	15
4.2.3 Electroanalytical performance of CPT-BDD reactor containing various concentrations of NVP.....	17
4.2.4 Application of the proposed method in real water samples	18
4.3 ELECTROCHEMICAL DYNAMICS OF APT-BDD REACTOR CONTAINING TNF AND QUANTIFICATION OF TNF	20

4.3.1	Electrochemical behavior of TNF on BDD reactor.....	20
4.3.2	Effect of electrolyte pH on BDD reactor containing 1.436 $\mu\text{g.mL}^{-1}$ of TNF drug.....	21
4.3.3	Electroanalytical performance of BDD reactor containing various concentrations of TNF.....	23
4.3.4	Application of the proposed method in real water samples.....	24
4.4	ELECTROCHEMICAL DETECTION OF EMTRICITABINE ON A MAGNETIC MOLECULARLY IMPRINTED POLYMER SENSOR.....	25
4.4.1	Electrochemical synthesis of magnetic non-imprinted and imprinted polymer sensor.....	25
4.4.2	Electrochemical characterization of the NIP/PABA- Fe_3O_4 /GCE and MIP/PABA- Fe_3O_4 /GCE.....	27
4.4.3	Electrochemical detection strategy for the quantification of FTC.....	29
4.4.4	Optimization studies of the parameters that influence the performance of the MMIP sensor.....	30
4.4.5	Analytical performance of Fe_3O_4 -MIP/GCE sensor.....	30
4.4.6	Interference, stability, repeatability, and reproducibility studies.....	31
	CHAPTER 5: CONCLUSIONS AND RECOMMENDATIONS.....	34
	REFERENCES.....	36

LIST OF FIGURES

Figure 2.1: Pathway of antiretroviral drugs in the aquatic environment	6
Figure 4.1: CV of CPT-BDD reactor in the absence (a) and the presence of 5 $\mu\text{g}\cdot\text{mL}^{-1}$ NVP (b) and its repeated scans (B) in 0.1 M PB (pH 12) at a scan rate of 50 $\text{mV}\cdot\text{s}^{-1}$ and potential window of 0-1.0 V.....	14
Figure 4.2: SWV of 5 $\mu\text{g}\cdot\text{mL}^{-1}$ NVP at different pHs (7-12) on CPT-BDD reactor (A). Regression plot of E_p vs pH from pH 7-10 and insert: regression plot of E_p vs pH from pH 10-12 (B).....	16
Figure 4.3: pH (pH 7-12) dependence of CPT-BDD reactor parameters for electro-oxidation of 5 $\mu\text{g}\cdot\text{mL}^{-1}$ of the drug in 0.1 M BR [Data plotted were obtained from Figure 4.2A and Table 4.2.	17
Figure 4.4: DPV response of a CPT-BDD reactor in 0.1 M PB (pH 12) containing various concentrations of NVP (0.1-50 $\mu\text{g}\cdot\text{mL}^{-1}$) (A). The corresponding calibration curve for the quantification of NVP (B).	18
Figure 4.5: Calibration curves for spiked wastewater (A) and tap water (B) samples on a CPT-BDD electrode	19
Figure 4.6: Cyclic voltammogram of BDD reactor in the absence (a) and the presence of 1.436 $\mu\text{g}\cdot\text{mL}^{-1}$ (b) TNF in 0.1 M Britton Robinson buffer (BR, pH 4) at a scan rate of 50 $\text{mV}\cdot\text{s}^{-1}$	20
Figure 4.7: Square wave voltammogram of 1.436 $\mu\text{g}\cdot\text{mL}^{-1}$ TNF at different pH (2-8) on BDD reactor (A). Regression plot E_p vs pH from pH 4-8; insert: Regression plot of E_p vs pH from pH 2-4 (B).....	22
Figure 4.8: pH (pH 2-8) dependence of BDD reactor parameters for electro-oxidation of 1.436 $\mu\text{g}\cdot\text{mL}^{-1}$ of TNF drug in 0.1 M BR [Data plotted were obtained from Figure 5.4A]	22
Figure 4.9: SWV of TNF at various concentrations (0.014-7.18 $\mu\text{g}\cdot\text{mL}^{-1}$) in an APT-BDD reactor containing 0.1 BR (pH 4). Insert: Enlargement of DPV at concentration range of 0.05-1.0 $\mu\text{g}\cdot\text{mL}^{-1}$	23
Figure 4.10: Calibration curve of spiked wastewater effluent (A) and tap water (B) samples.....	24
Figure 4.11: Electrochemical behavior of FTC on a bare GCE at a pH 2 and various scan rates (10-100 V) in the potential range of 0.0 to 2.2 V.	26
Figure 4.12: Cyclic voltammograms obtained for the electropolymerization of 5.0 mM PABA (A) and PABA-FTC (5:1) (B) in 0.1 M H_2SO_4 on a GCE at a scan rate of 50 $\text{mV}\cdot\text{s}^{-1}$ and potential window of -0.3 to 1.3 V using 7 CV scans. The arrows indicate the direction of the current as the number of cycles increases.	27
Figure 4.13: Cycle voltammograms of GCE, GCE/ Fe_3O_4 , PABA- Fe_3O_4 /GCE, NIP/ABA- Fe_3O_4 /GCE, and MIP/ABA- Fe_3O_4 /GCE in 0.1 M H_2SO_4 (A). Nyquist plot spectra of GCE, GCE/ Fe_3O_4 (a), PABA- Fe_3O_4 /GCE (b), NIP/ABA- Fe_3O_4 /GCE (c), MIP/ABA- Fe_3O_4 /GCE (d), MIP/ABA- Fe_3O_4 /GCE (extraction), (e) and MIP/ABA- Fe_3O_4 /GCE (rebinding) (f) in 0.1 M H_2SO_4 containing 1 mM $[\text{Fe}(\text{CN})_6]^{3-/4-}$. Conditions: -0.3 to 1.3 V, scan rate 50 $\text{mV}\cdot\text{s}^{-1}$, potential energy 0.5 V, frequencies 10 kHz to 1.0 Hz, amplitude 25 mV.....	28
Figure 4.14: SWV voltammetry of Fe_3O_4 -NIP/GCE and Fe_3O_4 -MIP/GCE in the presence and absence of FTC	29
Figure 4.15: DPV plots of MIP/PABA- Fe_3O_4 /GCE sensor during rebinding of different concentrations of the FTC template from 0.01 to 100 $\mu\text{g}\cdot\text{mL}^{-1}$ (A). Linear calibration curve for MIP/PABA- Fe_3O_4 /GCE at concentration range of 0.01 to 10 $\mu\text{g}\cdot\text{mL}^{-1}$ (B) and 1 to 100 $\mu\text{g}\cdot\text{mL}^{-1}$ (C).	31
Figure 4.16: Selectivity study of MIP/PABA- Fe_3O_4 /GCE (A) and NIP/PABA- Fe_3O_4 /GCE (B) in the presence of interfering species such as FTC, 3TC, EFV, TNF, NVP. Repeatability (C), reproducibility (D), and stability (insert D) studies of the MIP/PABA- Fe_3O_4 /GCE sensor.....	32

LIST OF TABLES

Table 2.1: Names and some physicochemical properties of the selected ARV.....	5
Table 2.2: Occurrence of the selected antiretroviral drugs in South African wastewater.....	7
Table 4.1: BDD reactor's electro-oxidation parameters for 5 $\mu\text{g}\cdot\text{mL}^{-1}$ NVP	15
Table 4.2: Effect of pH on electro-oxidation parameters of 5 $\mu\text{g}\cdot\text{mL}^{-1}$ NVP	17
Table 4.3: Regression plot data of the calibration curve obtained from square wave voltammetric analysis of NVP at various concentrations in the BDD reactor	18
Table 4.4: Recovery data of Zandvliet wastewater effluent sample spiked with NVP reference standard. Calibration curve method and DPV were used to obtain the information.....	19
Table 4.5: Recovery data of tap water sample spiked with NVP reference standard. Calibration curve method and DPV were used to obtain the information	19
Table 4.6: BDD reactor's electro-oxidation parameters for 1.436 $\mu\text{g}\cdot\text{mL}^{-1}$ TNF [Data obtained from Figure 4.6].....	21
Table 4.7: Effect of pH on electro-oxidation parameters of 1.436 $\mu\text{g}\cdot\text{mL}^{-1}$ TNF	22
Table 4.8: Regression plot data of the calibration curve obtained from DPV analysis of TNF at various concentrations in the APT-BDD reactor.	24
Table 4.9: Regression plot data of the calibration curve obtained from square wave voltammetric analysis of TNF at various concentrations in the BDD reactor.	25
Table 4.10: Recovery data of Zandvliet wastewater effluent sample spiked with TNF reference standard solution. The calibration curve method and DPV were used to obtain the information.....	25
Table 4.11: Recovery data of tap water spiked with TNF reference standard solution. The calibration curve method and DPV were used to obtain the information.....	25
Table 4.12: The charge resistance (R_{ct}) values of the different electrode material employed for sensor fabrication	28
Table 4.13: The changes in peak potential (E_p) and peak current (I_p) of the imprinted polymer in the presence and absence of FTC	29
Table 4.14: Selectivity and relative selectivity data of $\text{Fe}_3\text{O}_4\text{-MIP/GCE}$ and $\text{Fe}_3\text{O}_4\text{-NIP/GCE}$	33

ACRONYMS & ABBREVIATIONS

AIDS	Acquired immune deficiency syndrome
APT	Anodic pretreatment
ARV	Antiretroviral drugs
BDD	Boron doped diamond
CPT	Cathodic pretreatment
CV	Cyclic voltammetry/Cyclic voltammogram
E3Ps	Emerging persistent pharmaceutical pollutants
EFV	Efavirenz
EO	Electrooxidation
FTC	Emtricitabine
GCE	Glassy carbon electrode
HIV	Human immunodeficiency virus
LOD/Q	Limit of detection/quantification
MIP	Molecularly imprinted polymer
MMIP	Magnetic molecularly imprinted polymer
MOM	Magnitude of mineralisation current
MSS	Magnitude of sensing signal
NIP	Non-imprinted polymer
NVP	Nevirapine
OPM	Onset potential for mineralisation
OPS	Onset potential for sensing
SWV	Square wave voltammetry/Square wave voltammogram
TNF	Tenofovir
WWTP/s	Wastewater treatment plant/s

This page was intentionally left blank

CHAPTER 1: BACKGROUND

1.1 INTRODUCTION

Water is amongst the most essential natural resources required for life on earth. Its everyday functions include quenching thirst, food and drinks production, irrigation, and providing habitat to aquatic organisms. Although the earth is made up of 70% water, only about 2% is freshwater; the rest is seawater (98%) which is high in salinity and not suitable for humans and terrestrial ecosystem. According to UNICEF and WHO, more than 2.2 billion people lack access to safe and clean water and this number will increase due to the increase in population, water pollution, poor sanitation, and destruction of natural water sources (World Health Organization, 2019). By the year 2025, half of the world's population will be living in water-stressed areas (World Health Organization, 2019). Freshwater contamination is a worldwide crisis that requires an agent and efficient solutions. Over the years, freshwater sources have been contaminated by untreated wastewater effluents from domestic sewages, hospitals, industries, and agricultural run-offs. Inadequate or inappropriate management and treatment of wastewater and sanitation mean that the drinking water supplied to millions of people is chemically contaminated and may be dangerous to their lives. In 2017, there were at least 2 billion people whose drinking water sources were contaminated with faeces (World Health Organization, 2019). Contaminated water and poor sanitation have been linked to the transmission of diseases such as cholera, diarrhoea, hepatitis A, typhoid, and polio (World Health Organization, 2019).

One of the problems faced by South African wastewater treatment plants (WWTPs) and freshwater sources is the presence of emerging pharmaceutical pollutants, such as antiretroviral drugs (ARV) which are not removed by using conventional wastewater treatment techniques. ARV are medicinal drugs used in the treatment of infections caused by a retrovirus, called human immunodeficiency virus (HIV). The detection and removal of ARV and their metabolites in WWTPs and surface waters remain a major challenge in this century. Conventional wastewater treatment techniques such as activated sludge and biodegradation (Awaleh and Soubaneh, 2014) have been widely employed for their treatment in wastewater. However, these techniques are less efficient in removing most of these organic pollutants. Thus, they are discharged with wastewater effluent and accumulate in the environment as emerging persistent micropollutants. Due to the high HIV prevalence, high prescription rate, and high consumption rate in South Africa, ARV, and their metabolites have been detected at trace levels in WWTPs effluents (Prasse, Schlüsener et al., 2010; Schoeman, Mashiane et al., 2015; Wood, Duvenage et al., 2015; Funke, Prasse et al., 2016; K'oreje, Vergeynst et al., 2016; Ngumba, Gachanja et al., 2016; Ngumba, Kosunen et al., 2016; Schoeman, Dlamini et al., 2017; Abafe, Späth et al., 2018; Mosekiemang, Stander et al., 2019; Mlunguza, Ncube et al., 2020), surface waters (K'oreje, Demeestere et al., 2012; Aminot, Litrico et al., 2015; Wood, Duvenage et al., 2015; Funke, Prasse et al., 2016; K'oreje, Vergeynst et al., 2016; Boulard, Dierkes et al., 2018; Rimayi, Odusanya et al., 2018), groundwaters (Swanepoel, Bouwman et al., 2015; Fisher, Phillips et al., 2016; K'oreje, Vergeynst et al., 2016; Boulard, Dierkes et al., 2018; Rimayi, Odusanya et al., 2018), and even in drinking water (Dévier, Le Menach et al., 2013; Swanepoel, Bouwman et al., 2014; Funke, Prasse et al., 2016; Boulard, Dierkes et al., 2018).

Their occurrence in the aquatic environment does not only pollute the environment and interrupt the aquatic ecosystem, but also promotes the development of drug-resistant viruses and bacteria, leading to the development of new dangerous infections and diseases that may require new drugs for treatment (Ncube, Madikizela et al., 2018). Therefore, additional steps during wastewater treatment are required to avoid these secondary wastes. In most WWTPs, disinfection of the final WWTP effluent using chlorination and ultraviolet (UV) irradiation is common, however, these processes exhibit low oxidation and mineralization ability towards the recalcitrant organic pollutants.

Antiretroviral drugs exist at trace levels in the environment, so sensitive, precise, and accurate analytical methods are needed for monitoring these micropollutants in the environment. Of all analytical techniques used to monitor and quantify pharmaceuticals in wastewater and environment, liquid chromatography coupled with spectroscopic techniques (LC-MS/MS) and electrochemical sensors have shown to be more advantageous as detecting tools (Panditi, Batchu et al., 2013; Rossmann, Schubert et al., 2014; Sgobbi, Razzino et al., 2016; Sousa, Ribeiro et al., 2019). Indeed, liquid chromatography-mass spectroscopy hyphenated techniques have been very successful and effective in monitoring a wide range of pharmaceuticals in complex water samples. However, there are some challenges associated with them (Abafe, Späth et al., 2018; Mirzajani and Karimi, 2018). One of the drawbacks is the cost and the operational difficulties. On the other hand, electroanalysis (using sensors) is a very promising and efficient method for simultaneous detection of pharmaceuticals at low cost compared to chromatography/spectrophotometry. Therefore, this study explored the use of electrochemical methods for electroanalysis of the selected ARV in wastewater samples using.

For electro-oxidative sensing and mineralization of complex organic compounds such as ARV, electrochemical reactors cells that contain working electrodes that have very large potential windows are very necessary. This is because redox reactions occur at the electrode surface and that the oxidative decomposition of such calcitrant chemical materials requires very high potentials. Among various electrode materials used for electro-oxidation, the boron doped diamond (BDD) electrode has shown to be the best in mineralizing organic pollutants in the aquatic environment as compared to other anode materials such as IrO₂, RuO₂, SnO₂, Pt, and PbO₂. Moreover, the BDD electrode has shown to be the best in sensing pharmaceuticals in water compared to other carbon allotropes such as glassy carbon, graphite, carbon paste, graphene, carbon nanotubes, and carbon nanodots (Sousa, Ribeiro et al., 2019). BDD electrode is considered an ideal “non-active” electrode on which electrochemical oxidation of organics occurs very effectively. This is because it exhibits a wide usable electrochemical potential window (3.5 V), high resistivity to fouling, excellent reusability, low and stable background current signals, high corrosion resistance, relatively insensitive to dissolved oxygen, high thermal conductivity, and hardness, and chemically inertness (Macpherson, 2015; Feier, Gui et al., 2017). Moreover, modifying the electrode material with polymers and nanomaterials can enhance the performance of the electrochemical

1.2 AIMS

This project aimed at developing highly sensitive and selective electrochemical sensors for recalcitrant emerging contaminants such as ARV in municipal or domestic wastewater. Furthermore, the project aimed at developing a wireless bipolar electrochemistry-based reactor for the treatment of these contaminants in wastewater effluent.

1.3 OBJECTIVES

The objectives of the study were:

- To conduct a literature survey on the detection and removal of antiretroviral drugs in the environment
- To develop electrochemical sensors for the determination of the selected ARV in wastewater.
- To develop a wireless bipolar electrochemistry-based reactor for wastewater treatment.
- To write a final report on the findings of the study and present the work to the stakeholders and policymakers

1.4 SCOPE AND LIMITATIONS

The scope of the study entails:

- Studying the electrochemical behaviour of the selected Antiretroviral drugs on cathodically and anodically pre-treated boron-doped diamond electrode
- The development of electroanalytical methods for the determination of ARV in wastewater effluent and tap water samples
- The development of a bipolar electrochemical reactor for the degradation of these micropollutants in the environment

The limitations of this project include:

- Unavailability of resources. The instrument required for the bipolar electrochemical degradation of the drugs was not available.
- Time. A lot of time was lost during the Covid-19 pandemic, so some of the work was not covered due to time
- Accessing wastewater and surface water samples

CHAPTER 2: LITERATURE REVIEW

2.1 INTRODUCTION

This chapter provides literature regarding the overall research project. Firstly, the chapter explains what are antiretroviral drugs and why would they (fate) be detected in South African wastewater treatment plants and aquatic environments. This section also discusses electrochemical methods (voltammetry) as alternatives for the environmental monitoring of pharmaceuticals.

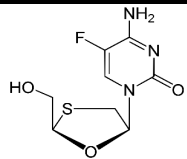
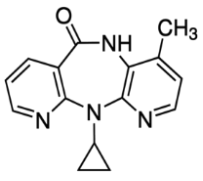
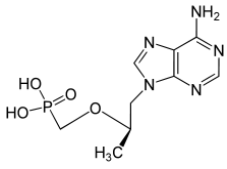
2.2 HIV/AIDS AND ANTIRETROVIRAL DRUGS IN SOUTH AFRICA

South Africa has the largest human immunodeficiency virus (HIV) epidemic in the world. In 2021, It was estimated that around 7.7 million people in South Africa were living with HIV and nearly more than half of them (4.4 million) were on antiretroviral therapy (ART) (Wood, Duvenage et al., 2015; Funke, Prasse et al., 2016; Schoeman, Dlamini et al., 2017; Abafe, Späth et al., 2018; Freer and Mudaly, 2022). HIV/AIDS is an infectious, deadly, and incurable disease, which in 2009 was estimated to have caused 350000 deaths in South Africa. Fortunately, South Africa has taken several measures towards reducing the rate of HIV-related infections among its population. The country is educating the people through HIV awareness programs, implementing the “90-90-90” HIV target program, providing ARV at low cost or free to HIV infected patients, and monitoring HIV-positive pregnant women to prevent mother-to-child HIV transmission (UNAIDS, 2017). Other remedial measures include the use of condoms, pre-exposure prophylaxis (PrEP) and medically suppressing the virus to prevent transmission. With the help of the largest antiretroviral therapy (ART) program in the world introduced in 1996, there has been a dramatic reduction in morbidity and mortality related to HIV infections

Antiretroviral drugs (ARV) or antiretroviral therapy (ART) are a group of medications used in the treatment of retroviral infections caused primarily by HIV type 1 and type 2 (Ncube, Madikizela et al., 2018). The ART works by suppressing the blood viral load below the detection limit (< 50 copies/mL) (Barletta, Edelman et al., 2004), thereby improving the immune system and the quality of life. The medication has reduced the number of HIV/AIDS-related death by more than 56% since 2004 (World Health Organization, 2018). Depending on their molecular mechanism and mode of action, ARV are categorised into six classes, namely; (Mosekiemang, Stander et al., 2019) non-nucleoside reverse transcriptase inhibitors (NNRTIs), protease inhibitors (PIs), integrase or strand transfer inhibitors (INI/INSTIs), Entry and fusion inhibitors (EFIs), and P450-3A inhibitors (Checa, Oliver et al., 2009; Asturias-Arribas, Delfino et al., 2016; Ncube, Madikizela et al., 2018; Rathbun, Lewis et al., 2019).

Each class targets a different phase of the retrovirus life cycle and helps the body fight the infections from multiple sites (Ross, Hendricks-Leukes et al., 2015; Pinto-Cardoso, Klatt et al., 2018). Hence, the drugs are given in combination. NRTIs and NNRTIs prevent the virus from replicating, PIs blocks viral protease enzyme, thereby preventing HIV deoxyribonucleic acid (DNA) from fragmenting into components required for the production of HIV ribonucleic acid (RNA) strands, INI/INSTIs stop the integrase (viral enzyme) from infecting the T-cells, and EFIs prevent the HIV from attaching or entering the DNA of the CD4 t-cells (Ncube, Madikizela et al., 2018) Although they are not regarded as ARV, P450-3A inhibitors are responsible for ARV metabolism, thereby increasing their efficacies. **Table 2.1** displays the physicochemical of the selected ARV for this study.

Table 2.1: Names and some physicochemical properties of the selected ARV

ARV	Class	Chemical structure (molecular weight)	Dosage (mg/day)	pKa (strong acid/base)	Log Kow; Water solubility (mg.mL ⁻¹)	Excreted (%) with faeces and/or urine	Ref.
Emtricitabine (FTC)	NRTI	 (247.248 g.mol ⁻¹)	200	2.65/14.25	-0.43, 112	86 (urine) 14 (faeces)	(Giri, Charan et al., 2014; Kurmi and Singh, 2017; Gautam, Lin et al., 2018; Kurmi, Sahu et al., 2020)
Nevirapine (NVP)	NNRTI	 (266.298 g.mol ⁻¹)	400	10.37/5.06	3.89, 0.0007046	10 (faeces) 83 (urine)	(DrugBank, 2005; Reis, de Assis et al., 2016; Eckhardt and Gulick, 2017)
Tenofovir disoproxil fumarate (TDF/TNF)	NRTI	 (287.213 g.mol ⁻¹)	300	3.75/6.7	1.25; 13.4	31.7 (faeces) <1 (urine)	(Medscape, 1994-2021; DrugBank, 2005; Panhard, Legrand et al., 2007; Golla, Kurmi et al., 2016)

2.3 ANTIRETROVIRAL DRUGS IN WASTEWATER AND AQUATIC ENVIRONMENT

2.3.1 The fate of antiretroviral drugs in wastewater

The increase in the production and consumption of ARV for the treatment of growing HIV infections has resulted in the fate and presence of these emerging organic pollutants in the aquatic environment. After oral administration and digestion by the human system, ARV may either be partially or completely metabolised into pharmacologically active metabolites and excreted with biological excreta (i.e. urine and faeces) into domestic sewage systems (Zhou, Chen et al., 2015; Abafe, Späth et al., 2018; Ncube, Madikizela et al., 2018; Nannou, Ofrydopoulou et al., 2019; Zhou, Wang et al., 2019; Mlunguza, Ncube et al., 2020). As depicted in **Figure 2.1**, ARV primarily enters the aquatic environment through wastewater from hospitals, pharmaceutical production industries, and domestic sewages of end-users and accumulates in surface water (Aminot, Litrico et al., 2015;

Schoeman, Mashiane et al., 2015; Wood, Duvenage et al., 2015; Funke, Prasse et al., 2016; K'oreje, Vergeynst et al., 2016; Wooding, Rohwer et al., 2017; Boulard, Dierkes et al., 2018; Rimayi, Odusanya et al., 2018; Horn, Vogt et al., 2022), drinking water (Swanepoel, Bouwman et al., 2015; Wood, Duvenage et al., 2015; Furlong, Batt et al., 2017; Boulard, Dierkes et al., 2018), groundwater (Swanepoel, Bouwman et al., 2014; Swanepoel, Bouwman et al., 2015; K'oreje, Vergeynst et al., 2016; Boulard, Dierkes et al., 2018; Rimayi, Odusanya et al., 2018), soil (Al-Rajab, Sabourin et al., 2010; Schoeman, Dlamini et al., 2017) and even plants (Mlunguza, Ncube et al., 2020). Since most ARV are reluctant against conventional wastewater treatment processes; they are continuously discharged and accumulated into nearby water bodies through wastewater effluents. The other pathway that ARV uses to enter the aquatic environment is through their improper and illegal disposal into water sources and land (Nannou, Kosma et al., 2015).

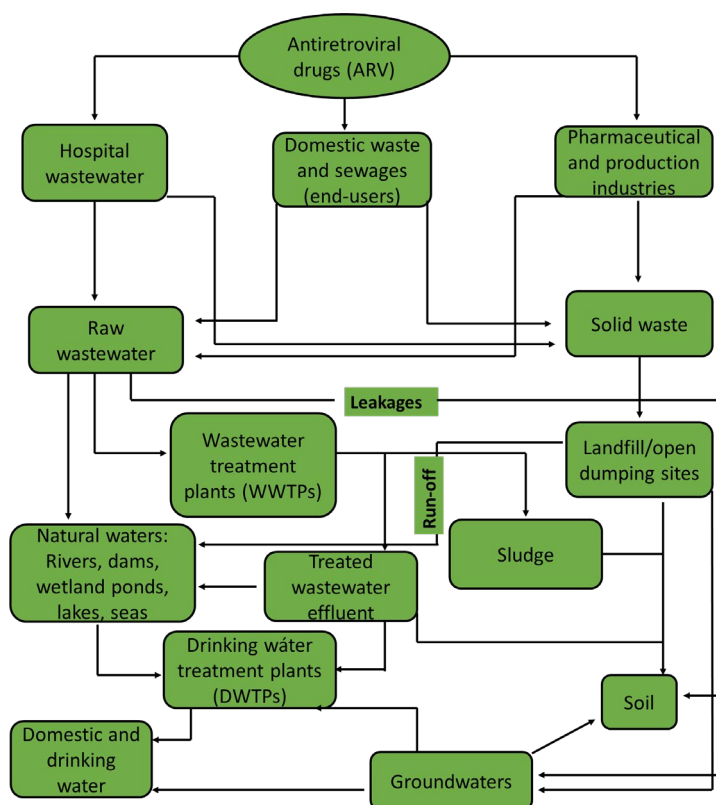


Figure 2.1: Pathway of antiretroviral drugs in the aquatic environment

2.3.2 Occurrence of antiretroviral drugs in wastewater

The occurrence of ARV in the South African aquatic environment is due to the high HIV prevalence and the implementation of the largest ARV program in the country. **Table 2.2** depicts the concentrations of the selected ARV in South African wastewater influent and effluent. The frequently detected ARV in the wastewater are NVP, ABV, ZDV, EFV, TNF, 3TC, and FTC. Mlunguza et al. (Mlunguza, Ncube et al., 2020) monitored the presence of FTC, EFV, and TNF in the Amanzimtoti WWTP influents and effluents using high-pressure liquid chromatography-mass tandem spectroscopy (HPLC-MS/MS). TNF was detected at a concentration of $0.25 \pm 2.4 \mu\text{g.L}^{-1}$ in the influent, while the compound was not quantified in the effluent. This was because the drug existed at a concentration lower than the limit of quantification (<LOQ) of the instrument (Mlunguza, Ncube et al., 2020). This indicates that a certain amount of TNF was removed or converted to a different metabolite during wastewater treatment processes. For FTC, concentrations of up to $3.10 \pm 3.1 \mu\text{g.L}^{-1}$ were reported in the WWTP influent, whereas the effluent contained $0.22 \pm 2.1 \mu\text{g.L}^{-1}$ (Mlunguza, Ncube et al., 2020). This shows that about 70% of the drug was removed by the conventional method used. The author further detected the drug in the roots, leaves, and stem of a water hyacinth plant at a concentration of 11.7 ± 0.52 , 3.91 ± 0.002 ,

and $1.05 \pm 0.24 \mu\text{g.kg}^{-1}$, respectively (Mlunguza, Ncube et al., 2020). A concentration of up to $172 \mu\text{g.L}^{-1}$ of FTC was detected by Mosekiemang et al. (Mosekiemang, Stander et al., 2019) in the Western Cape WWTP influent. Fortunately, about 97% of it was removed during biological and membrane bioreactor treatment. The chlorination treatment resulted in 76% removal.

Table 2.2: Occurrence of the selected antiretroviral drugs in South African wastewater

Antiretroviral drugs	Occurrence (ng.L^{-1})		Region/country	Ref.
	Influents	Effluents		
FTC	172	41.7	Western Cape	(Mosekiemang, Stander et al., 2019)
FTC	31.30	<LOQ (919)	Western Cape	(Mosekiemang, Stander et al., 2019)
FTC	3100 ± 3.1	220 ± 2.1	Amanzimtoti WWTP, KZN	(Mlunguza, Ncube et al., 2020)
FTC	300 ± 0.3	220 ± 0.1	Northern WWTP, KZN	(Mlunguza, Ncube et al., 2020)
FTC	1470 ± 0.1	350 ± 0.1	Umbilo WWTP, KZN	(Mlunguza, Ncube et al., 2020)
FTC	<LOQ	110 ± 3.0	Umhlatuzana, KZN	(Mlunguza, Ncube et al., 2020)
NVP	2100 ± 150	1900 ± 68	DEWATS, KZN	(Abafe, Späth et al., 2018)
NVP	670 ± 23	540 ± 34	Northern KZN	(Abafe, Späth et al., 2018)
NVP	2800 ± 190	1400 ± 63	Phoenix, KZN	(Abafe, Späth et al., 2018)
NVP	681	764	Western Cape	(Mosekiemang, Stander et al., 2019)
NVP	n/a	92-473	Southern Gauteng	(Schoeman, Dlamini et al., 2017)
NVP	2100	350	Vereeniging	(Schoeman, Mashiane et al., 2015)
TNF	170 ± 2.6	Nd	Northern WWTP, KZN	(Mlunguza, Ncube et al., 2020)
TNF	<LOQ	<LOQ	Umbilo WWTP	(Mlunguza, Ncube et al., 2020)
TNF	100 ± 1.1	<LOQ	Umhlatuzana	(Mlunguza, Ncube et al., 2020)

KZN: KwaZulu-Natal; n/a: not applicable, LOQ: Limit of quantification

The low concentration of $0.98 \pm 0.05 \mu\text{g.mL}^{-1}$ FTC recorded by Funke et al. (Funke, Prasse et al., 2016) is understandable, as the use of ARV in Germany is not as high compared to South Africa. However, Funke et al. (Funke, Prasse et al., 2016) also detected the transformation products carboxy-emtricitabine (COOH-FTC) and the emtricitabine S-oxide (FTC-S-Oxide) at concentrations of 0.48 ± 0.059 and $0.068 \pm 0.007 \mu\text{g.L}^{-1}$, respectively. As an alternative to FTC, 3TC is also an ARV that is widely used in South Africa and Africa. The presence of 3TC in South Africa was monitored only by Mosekiemang et al. (Mosekiemang, Stander et al., 2019) and was detected at a concentration of $20.9 \mu\text{g.L}^{-1}$ in the influent, while its presence in the effluent was not quantifiable (<LOQ). The highest concentrations of 3TC in wastewater were mostly recorded in Kenya, as this drug is part of the first-line daily dose ARV regimen that is widely used in the country for the treatment of HIV (Ngumba, Gachanja et al., 2016; Abafe, Späth et al., 2018). As part of the daily dose HIV regimen used in South Africa, EFV has been extensively detected in the wastewater influent and effluent. EFV is the most abundant drug with a concentration of up to $37.3 \mu\text{g.L}^{-1}$ in the Northern WWTP effluent and up to $26.3 \mu\text{g.L}^{-1}$ in the WWTP influent (Mlunguza, Ncube et al., 2020). However, they found these results strange as EFV has low water solubility than FTC and TNF. The low solubility of EFV means that it can easily adsorb onto the solid particles and be removed with the activated sludge. Nonetheless, similar results were observed by Abafe et al. (Abafe, Späth et al., 2018), with WWTP influent containing $24 \mu\text{g.L}^{-1}$ and effluent containing $33 \mu\text{g.L}^{-1}$ of EFV (Abafe, Späth et al., 2018). However, Schoeman (Schoeman, Dlamini et al., 2017), K'Oreje (K'Oreje, Vergeynst et al., 2016), and Mosekiemang (Mosekiemang, Stander et al., 2019) reported a decrease in the concentration of EFV after conventional treatment although it was <50%.

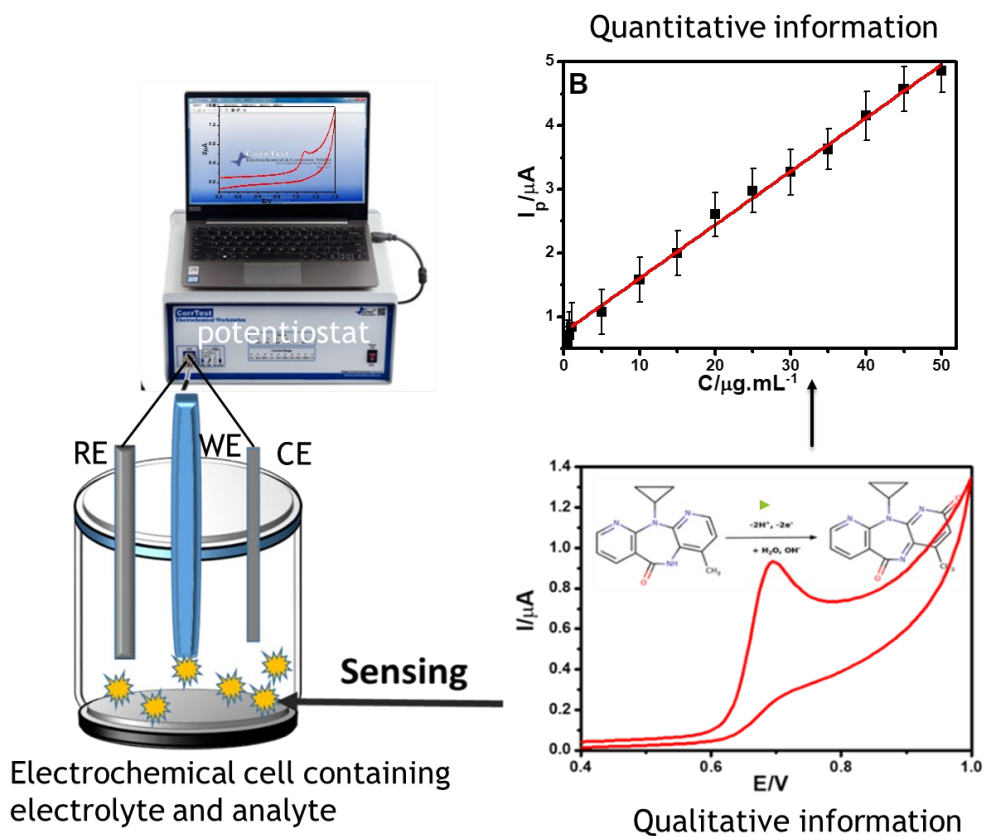
2.4 ELECTROANALYSIS AND ELECTROCHEMICAL SENSORS

Electrochemical or electroanalytical methods are analytical methods that use electrical stimulation to study an analyte's chemical reactivity and to determine its concentration in solution. They are the second major category of instruments used in analytical chemistry. Electrochemical sensors are portable, sensitive, miniaturisable, easy-to-use, cost-effective, and non-lab-based analytical tools that use small sample volumes during the detection of the analyte (i.e. ARV) in wastewater and biological samples (Sanvicens, Mannelli et al., 2011; Nagaraj, Jacobs et al., 2014; Veseli, Mullallari et al., 2019). These analytical devices use an electrically conducting probe, called electrodes to make electrical contact with the analyte in solution. The electrodes are used in conjunction with electric or electronic devices called potentiostat, which measures the electrical signal generated during the interaction of the analyte with the electrode. The measured electrical parameter is related to the identity of the analyte or its quantity in the solution. Depending on the electroanalytical method used, the potentiostat can either apply current or potential to the electrodes in solution to initiate electron flow between the analyte dissolved in the solution and the electrode immersed in the solution. Usually, electrochemical sensors use two or more electrodes immersed in a conducting solution called an electrolyte.

An electrolyte is a conductive solution with a lot of ions that allow charge transportation. The first electrode is called the working electrode (WE), which is usually made up of a conducting material. This is the electrode where the electrochemical reactions occur. The second electrode is the counter or auxiliary electrode (CE) usually a platinum wire. This electrode completes the electrical circuit and allows charge (current) to flow in the circuit. The third electrode is called the reference electrode (RE) and it is used to measure and control the potential of the WE electrode without passing a current through it. The most common reference electrodes are silver/silver chloride (Ag/AgCl) and saturated calomel electrode (SCE). Depending on the electrical parameter that is measured, electrochemical methods can be categorized into five main methods, namely; amperometry, voltammetry, potentiometry, coulometry, and electrochemical impedance spectroscopy (EIS). As the name implies, amperometry monitors the electrical current (measured in Ampere) of the working electrode as it interacts with the analyte in solution, while the potential is kept constant. Voltammetry is a branch of amperometry that measures the electrical current of the working electrode while the potential is varied in a regular manner.

Electrochemical impedance monitors the charge resistance transfer (R_{ct}) of the WE at a constant potential and varied frequencies. Coulometry measures the quantity of electrical charge (Coulombs) that is required to complete a reaction at the surface of the electrode. Potentiometry involves measuring the potential between two electrodes while the electrical current is controlled. This project focused more on voltammetric techniques as they are most dominant in the electroanalysis of pharmaceuticals. Moreover, they are very sensitive, easy to use and understand, have short analysis time, and also provide both qualitative and quantitative information about the analyte of interest.

It is worth noting the type of material used on the working electrode as it has an impact on the sensitivity and selectivity of the electroanalytical method. The commonly used electrodes in electroanalysis are glassy carbon electrode (GCE), boron-doped diamond (BDD) electrode, gold electrode, and indium tin oxide electrode (ITO). In most cases, these conventional electrodes are chemically modified with conductive materials such as polymers, metals, nanomaterials, and also with biological material. Biological materials are usually used to improve the selectivity of the sensor while conducting polymers and nanomaterials improve the selectivity, sensitivity, and overall performance of the sensor. Although there is no published work on electroanalysis of ARV in wastewater and surface water samples, there are studies on the voltammetric analysis of other micropollutants in wastewater and surface water (Lahcen, Baleg et al., 2017; Feier, Florea et al., 2018; AL-Ammari, Ganash et al., 2019; Ayankojo, Reut et al., 2020; Rebelo, Pacheco et al., 2020; Kokulnathan, Kumar et al., 2021; Rebelo, Costa-Rama et al., 2021). The diagram in **Scheme 2.1** shows a schematic diagram of the components used in the electroanalysis of ARV and the produced voltammetric signal for one of the drugs studied. The diagram shows both the qualitative and quantitative results obtained using the voltammetric method.



Scheme 2-1: Schematic diagram of the components used in electrochemical sensors and the information that can be obtained from the analytical method

CHAPTER 3: MATERIALS AND METHODS

3.1 INTRODUCTION

This chapter provides detailed information on the chemical and reagent, experimental methodology used to prepare the sensors, and the instruments used for electroanalysis of the antiretroviral drugs. The electrochemical behaviour of NVP and TNF were studied at different pH values using SWV and CV and their electrooxidation parameters were recorded. For NVP qualitative and quantitative analysis, a cathodically pretreated boron-doped diamond electrode (CPT-BDD) was used, while for TNF analysis an anodically pretreated boron-doped diamond electrode (APT-BDD) was employed. Electroanalysis of FTC was performed on a magnetic molecularly imprinted electrochemical sensor. The experiments were done in triplicates ($n = 3$) and the relative standard deviation (%) was calculated. Before analysis of any of the drugs, the electrochemical response of the electrode in the absence of the analyte was recorded six times, and the data was used to calculate the standard deviation of the blank which was used in determining the LOD and LOQ of the developed electroanalytical methods for ARV analysis.

3.2 CHEMICALS AND REAGENTS

The reference standards of efavirenz, emtricitabine, nevirapine and tenofovir were purchased from Sigma Aldrich, South Africa. Sodium phosphate monobasic (NaH_2PO_4), sodium phosphate dibasic (Na_2HPO_4), sodium hydroxide (NaOH), hydrochloric acid (HCl), sodium acetate (NaCH_2COOH), acetic acid (CH_2COOH), boric acid (H_3BO_3), phosphoric acid (H_3PO_4), and sulphuric acid (H_2SO_4), sulphuric acid (H_2SO_4), para-aminobenzoic acid (PABA), Iron (III) chloride hexahydrate ($\text{FeCl}_3 \cdot 6\text{H}_2\text{O}$), sodium acetate (NaCH_3COO), ethylene glycol, were also purchased from Sigma-Aldrich and used as received. NaCH_2COOH and CH_2COOH were used to prepare acetate buffer (0.1 M AceB), H_3BO_3 , H_3PO_4 , and CH_2COOH were used to prepare Britton-Robinson buffer (0.1 M BR), and NaH_2PO_4 and Na_2HPO_4 were used to prepare the phosphate buffer (0.1 M PB). NaOH (1.0 M) and HCl (1.0 M) were used to adjust the pH of the buffers. All solutions were prepared using ultrapure water (resistivity not less than 18 M Ω cm) obtained from the Milli-Q Direct-0.3 purification system. All the experiments were carried out at room temperature and the solutions were bubbled using nitrogen gas for 5 min before running the electrochemical measurements. The magnetite iron oxide nanoparticles (Fe_2O_4 NPs) were synthesized using the modified solvothermal method reported by Kozokova et al. (Kozakova, Kuritka et al., 2015). Briefly, 5 mmol $\text{FeCl}_3 \cdot 6\text{H}_2\text{O}$ (1.352 g) and 50 mmol NaCH_3OO (4.101 g) were dissolved in 60 mL ethylene glycol. The homogenous yellowish-brown mixture solution was stirred for 30 min at 300 rpm and then it was transferred into a 100 mL microwave Teflon tube. The solution was then subjected to microwave heating at 200°C and 900 W for a fixed duration of 10 min. The pressure evolved in the vessel during microwave-solvothermal reaction was 60 bars. Post synthesis, the black colloidal dispersion was cooled at room temperature and the magnetic black precipitate was collected with the help of an external permanent magnet. The precipitate was further washed several times with deionized water and absolute ethanol to remove the unreacted chemicals. Finally, the washed product was dried in an oven at 60°C for modification of the Fe_2O_4 NPs with PABA, 1 mg.mL⁻¹ of the nanoparticles suspended in ethanol was mixed with 1 mM PABA and the solution was stirred for 3 h to allow the interaction between the oxygen group of the nanoparticles and the hydrogen and nitrogen groups of PABA.

3.3 INSTRUMENTATION

For conventional electrochemical experiments, a boron-doped diamond (BDD) reactor was constructed with a BDD electrode (diameter of 3 mm, Windsor Scientific) as the working electrode, Ag/AgCl (3M NaCl type) reference electrode, and a platinum wire as the counter electrode. For analysis of emtricitabine, a glassy carbon electrode (GCE) was used. The electrodes were contained in glass vessels (10 mL) with an appropriate electrolyte. The three electrodes were connected to appropriate slots in portable PalmSens potentiostat with a dc-potential range of ± 10 V, maximum current ± 30 mA, and maximum data acquisition rate of 150,000 data points/s and potentiostatic current range of 100 pA-10 mA work station made of a three-electrode system setup. Cyclic voltammetry (CV), square wave voltammetry (SWV), differential pulse voltammetry (DPV), and electrochemical impedance spectroscopy (EIS) were used as the electrochemical techniques for the experiments. The pH values of the samples were measured by Hanna 221 pH meter (Hanna Instruments, USA)

3.4 ELECTROCHEMICAL PROCEDURE

3.4.1 Preparation of the BDD working electrode

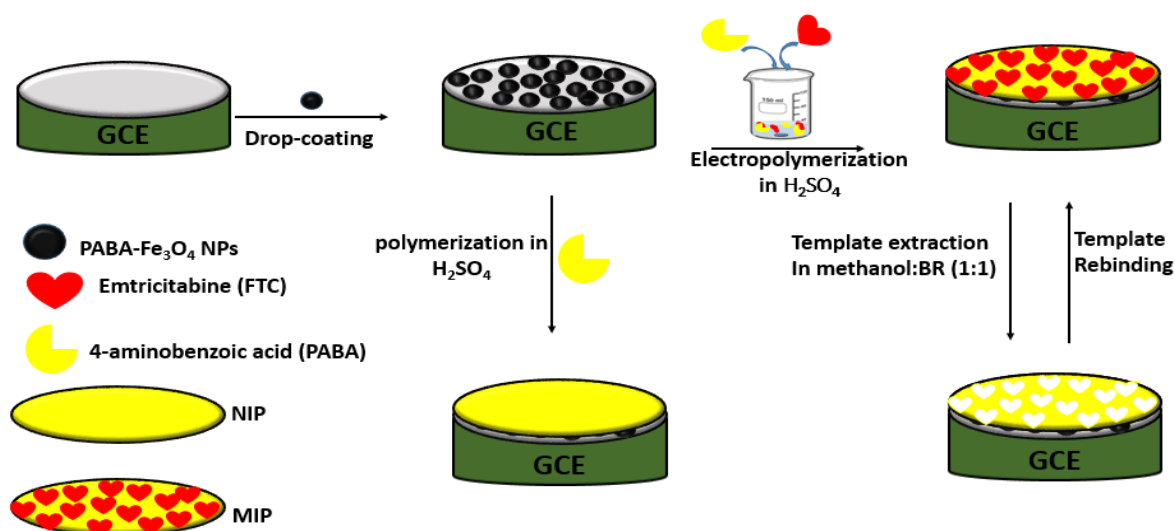
The BDD working electrode was cleaned by first polishing using 1.0, 0.3, and 0.05 μm alumina powder, washed with water, and sonicated in 1:1 water and ethanol for 10 min. Before electrochemical measurement, the BDD was electrochemically activated in 0.5 M sulphuric acid (H_2SO_4) by applying a potential of -2.0 V vs Ag/AgCl (cathodic pre-treatment) or + 2.0 V vs Ag/AgCl (anodic pre-treatment) for 120 s before each measurement. The BDD reactor cell contained the three electrodes and either of the appropriate buffers were used as electrolytes. A predetermined amount of NVP or TNF was added to the cell solution and a pH meter was used to monitor the pH of the drug solutions before and after analysis. The cell solution was purged with nitrogen gas for 5 min before performing experiments. CV SWV and DPV were recorded at 0-1.0 V potential windows for NVP analysis and 0-1.8 V for TNF. SWV measurements were carried out at frequency (f) of 10 Hz, step potential (Estep) 5 mV, and amplitude (A) of 25 mV. The voltammograms were also analysed to determine the reactor's electro-oxidation parameter. The experiments were repeated 3 times (n=3) and the relative standard deviation was determined using the peak current (I_p) values.

3.4.2 Electrochemical synthesis of magnetic molecularly imprinted polymer (MMIP) and non-imprinted polymer (MNIP) for FTC determination

Prior to the preparation of (MMIP) and MNIP sensor, the Fe_3O_4 NPs surface was modified with PABA. This was done to prevent magnetostatic interactions and aggregation caused by the anisotropic dipole attractions, which subsequently deactivate the catalytic activity of the Fe_3O_4 NPs via dimerization (Esam, Akhavan et al., 2020). Moreover, coating the layer of the nanoparticles also works as the connecting bridge between the electrode, magnetite, polymer, and the analyte through π - π stacking interactions and hydrogen bonding. For this purpose, 5 mg of dry Fe_3O_4 NPs were dispersed in 10 mL ethanol and sonicated for 30 min. Thereafter, 5.0 mM PABA was added to the reaction mixture that was further sonicated for 3 h to allow the bonding between the nanoparticles and the PABA. Finally, the modified nanoparticles (PABA- Fe_3O_4 NPs) were separated from the solution using an external magnet and washed with water to remove the unbound PABA. For the preparation of the MMIP, 5.0 mM PABA and 1.0 mM FTC (5:1) were mixed and stirred for 10 min in a degassed 0.1 M H_2SO_4 electrolyte to allow compounds interaction and bonds formation. Thereafter, the prepared mixture was added to the modified nanoparticles (5:1:2). The pre-polymerization solution was further stirred for 10 min and then electropolymerised on a GCE using seven (7) consecutive cyclic voltammetric scans in the potential range -0.3 to +1.3 V and a scan rate of 50 $\text{mV}\cdot\text{s}^{-1}$. The GCE was first thoroughly cleaned and then electrochemically pretreated in 0.5 M H_2SO_4 using 10 cyclic scans in the potential window of -1.5 to 1.5 V at 100 $\text{mV}\cdot\text{s}^{-1}$.

The MNIP was prepared in the same manner, except that the template (FTC) was not added. The prepared platforms were named MIP/PABA-Fe₃O₄/GCE and NIP/PABA-Fe₃O₄/GCE. The stock solution of FTC was prepared in deionized water, while the monomer was prepared in ethyl acetate. The fabricated MIP/PABA-Fe₃O₄/GCE and NIP/PABA-Fe₃O₄/GCE sensors were washed with a mixture of acetic acid and methanol mixture (1:1) for 10 min (as the optimal template extraction time) to remove the template and check the effect of eluent on the polymer. The developed sensors were stored at ambient temperature and their stability over time was investigated.

Scheme 3-1 present the graphical representation of the electrochemical sensor preparation.



Scheme 3-1: Schematic diagram for the preparation of NIP/PABA-Fe₃O₄/GCE and MIP/PABA-Fe₃O₄/GCE

3.5 PREPARATION OF WATER SAMPLES

Wastewater effluent samples were collected from the Zandvliet wastewater treatment plant, Cape Town, South Africa, while tap water samples were collected from the University of the Western Cape, South Africa. The Zandvliet WWTP treat wastewater from the southern part of Kuils River, Delft, Blackheath, Blackheath industries, Blue Downs, Eersteriver, De Wijnlanden, Thembokwezi, Mxolisi, Phetane, and Khayelitsha. The WWTP is currently treating 72 million litres per day (MI/d) of wastewater, and it is expected to treat a capacity of 80 MI/d by June 2023. The treatment work currently uses the conventional biological activated sludge as the wastewater treatment process, and it also has the membrane bioreactor module technology which is used for solid and liquid separation (African News Agency and Independent Online (IOL), 2019; ZUTARI, 2021). Tap water was collected from SensorLab, Chemistry Department University of the Western Cape, South Africa.

The wastewater samples were collected in amber glass bottles and stored in the refrigerator when not in use. For real sample analysis, wastewater effluent was mixed with the appropriate electrolyte solution. During analysis, the wastewater solution was spiked with known concentrations of the pure reference standard (either NVP, TNF, or FTC) and analysed for the traces of the analyte. The same method was applied in tap water analysis, except that the electrolyte was prepared using tap water instead of deionized water. The concentration or amount of analyte in the real samples was determined by the calibrationcurve method and the analysis was carried out three times (n=3) and a relative standard deviation (%) was calculated using the standard deviation of the three results and their mean.

CHAPTER 4: RESULTS AND DISCUSSIONS

4.1 INTRODUCTION

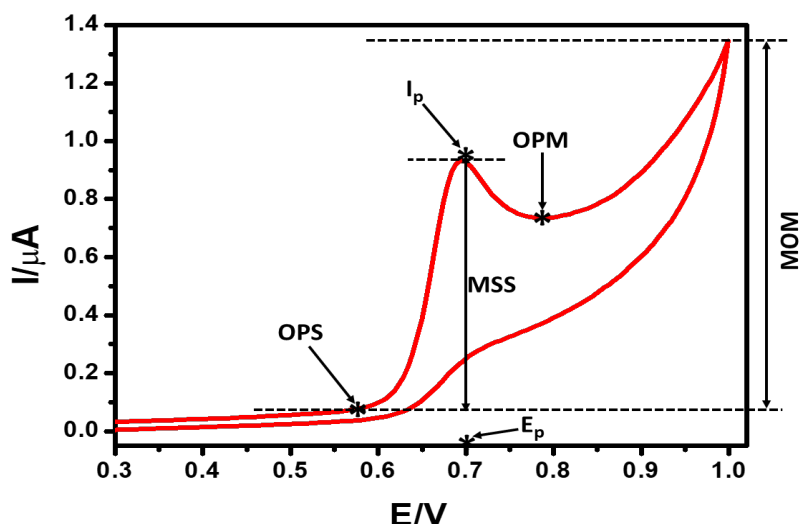
This section provides results and discussions on the qualitative and quantitative electroanalysis of NVP, TNF, and FTC. The chapter is divided into three sub-headings. The first heading deals with qualitative and quantitative analysis of NVP on CPT-BDD, the second heading involves qualitative and quantitative analysis of TNF on an APT-BDD, and the last heading deals with quantitative analysis of FTC on a magnetic molecularly imprinted electrochemical sensor. Every result or figure presented has its discussion above it. Due to their different physicochemical properties, the selected ARV behaved differently from each other. NVP was not electroactive in acidic media, and TNF was more electroactive in acidic media. According to the CV and SWV obtained for all the drugs, it shows that these ARV are irreversibly oxidized and their peak potential and current are affected by the pH of the solution. For real water sample analysis, the samples were spiked with a known concentration of the reference standard ($\mu\text{g}\cdot\text{mL}^{-1}$), and the recoveries of the drugs were determined.

4.2 ELECTRO-OXIDATION AND ANALYSIS OF NVP DRUG ON A BDD REACTOR

For successful sensing and mineralization of ARV in wastewater, one needs to understand the nature and behaviour of ARV electrochemical processes at the BDD reactor surface. CV and SWV were used to investigate the influence of scan rate (ν), pH, and electrolyte composition on the position, intensity, and morphology of NVP signals at the BDD reactor. As part of the analysis for direct current (DC) voltammetry results, the following reactor's parameters for the ARV were evaluated; onset potential for sensing (OPS), onset potential for mineralization (OPM) peak potential (E_p), magnitude of sensing signal (MSS) and magnitude of mineralization and oxidation (MOM). The OPS represents the potential at which the oxidation of the drug commences, while the MSS represents the magnitude of the sensing signal. E_p is the peak potential that is required for sensing the ARV and complete conversion of the drug to its oxidised form. The OPM represents the potential at which the organic material starts to undergo complete electro-incineration into carbon dioxide (CO_2), water (H_2O), and ammonia (NH_3), whereas MOM represents the total current produced by the complete decomposition or mineralization of the organic compound. A typical cyclic voltammogram in **Scheme 4-1** depicts all the electro-oxidation parameters of the ARV in the BDD reactor.

4.2.1 Electrochemical dynamics of NVP at the BDD reactor

Cyclic voltammetry measurements were carried out to evaluate the electrochemical behaviour of $5 \mu\text{g}\cdot\text{mL}^{-1}$ NVP on a cathodically pretreated (CPT) BDD reactor in the presence of 0.1 M PB (pH 12) electrolyte. The CV was carried out at a potential range of 0-1.0 V (vs. Ag/AgCl) and a scan rate of $50 \text{ mV}\cdot\text{s}^{-1}$. In the chosen potential range and as depicted in **Figure 4.1(A, B)**, NVP exhibits one well-defined irreversible oxidation peak at approximately 0.67 V vs Ag/AgCl. This peak is due to electro-oxidation of NVP at alkaline conditions. In basic conditions, the pyridine group of the NVP is rapidly deprotonated to allow hydroxylation of the molecule before electro-oxidation. After hydroxylation, the molecule then undergoes electro-oxidation to produce a quinone imine. The electro-oxidation parameters of NVP at the CPT-BDD reactor are listed in **Table 4.1**. At the low potential of 0.604 V (OPS), the BDD reactor can sense NVP in the electrolyte and at the potential of 0.67 V, NVP is oxidised into its products with an intensity (MSS) of $0.938 \mu\text{A}$. NVP electro-oxidation by-products start to mineralise into CO_2 , NH_3 , and H_2O at 0.738 V (MOM). At the studied potential range, its MSS was $1.240 \mu\text{A}$. The sensitivity of the BDD reactor towards NVP was $0.44 \mu\text{A}/\mu\text{g}\cdot\text{mL}^{-1}$.



Scheme 4-1: Schematic diagram of a typical CV of an ARV drug (NVP) response in the BDD reactor depicting the electrooxidation parameters; onset potential for sensing (OPS), oxidation peak potential (E_p) and peak current (I_p), onset potential for mineralisation (OPM), magnitude of sensing signal (MSS), and magnitude of mineralisation and oxidation (MOM).

In addition, the repeatability of the BDD reactor was carried out by performing subsequent five (5) scans at the same conditions (**Figure 4.1B**). The peak current of NVP decreased from scan 1-3, then stabilised at higher scans. This can be due to the weak interactions between the NVP electro-oxidised product (quinone imine) and the cathodically pretreated BDD. Since BDD is resistant to fouling and easy to clean, there were limited possibilities for the by-products to adsorb on the electrode surface. In addition, cathodically pretreated BDD enhances resistance to fouling, while increasing the signal of the electro-active species [19-21].

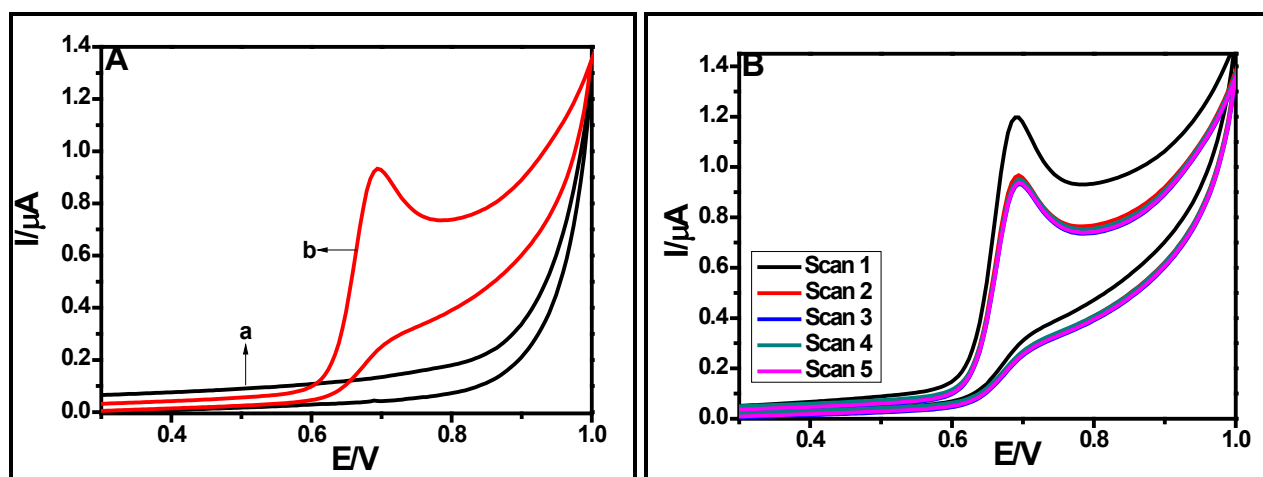


Figure 4.1: CV of CPT-BDD reactor in the absence (a) and the presence of $5 \mu\text{g.mL}^{-1}$ NVP (b) and its repeated scans (B) in 0.1 M PB (pH 12) at a scan rate of 50 mV.s^{-1} and potential window of 0-1.0 V.

Table 4.1: BDD reactor's electro-oxidation parameters for 5 µg.mL⁻¹ NVP

Parameters	Values
Onset potential for sensing (OPS)	0.604 V
Peak current (magnitude of sensing signal, MSS)	0.938 µA
Peak potential (E _p)	0.67V
Onset potential for mineralization/Decomposition (OPM)	0.738 V
Magnitude of mineralization (MOM)	1.240 µA
Sensitivity (MSS/[NVP])	0.019 µA/ µg.mL ⁻¹
Relative standard deviation (RSD)	1.6%

4.2.2 Effect of pH on electro-oxidation parameters of NVP at the BDD reactor

The pH of the supporting electrolyte affects the position, height, and morphology of the resulting signal of an electroactive compound, especially drugs since protons are involved in the reaction. Moreover, varying the pH of the supporting electrolyte during electro-oxidation of an electroactive compound can provide significant information about the mechanisms involved. Therefore, the pH dependency of electro-oxidation of 5 µg.mL⁻¹ NVP through BDD reactor was investigated using SWV in the pH range of 2-12 of 0.1 M PB electrolyte. From the studies pH range, NVP was only electro-oxidised at pH > 6, as there was no oxidation or reduction peak at pH 2-6 in the potential range of 0.0-1.2 V.

Figure 4.2A, displays the differential pulse voltammograms of NVP at various pH values, while **Figure 4.2B** and insert depicts the regression curves of NVP at pH 7-10 and pH 10-12, respectively. The regression curves had the following equations:

$$E_{pa} \text{ (V)} = -0.0354 \text{ pH} + 1.0883 \text{ (R}^2 = 0.914\text{); (pH 7-10)} \quad [4.1]$$

$$E_{pa} \text{ (V)} = -0.0510 \text{ pH} + 1.24998 \text{ (R}^2 = 1\text{); (pH 10-12)} \quad [4.2]$$

A slope of -0.0510 V.pH⁻¹ in Equation 4.2, which is closer to the Nernstian value of -0.059 V.pH⁻¹, suggests that an equal number of protons and electrons were involved in the electro-oxidation of NVP at the BDD reactor. While the slope of -0.0354 V.pH⁻¹ in Equation 4.1 suggests unequal numbers (Gholivand, Ahmadi et al., 2017; Ahmadi, Eyvani et al., 2019). In addition, the intersection of E_p vs pH for the two regression curves is at 10.36, which is closer to the theoretical pK_a of 10.37 for NVP (DrugBank, 2005; Gholivand, Ahmadi et al., 2017; Ahmadi, Eyvani et al., 2019). At pH < 6, the nitrogen on NVP is positively charged and still not protonated at pH 6-10. At pH > 10, the molecule will start gaining negative charges allowing protons to take part during electro-oxidation of NVP (chemicalize.org, Gholivand, Ahmadi et al., 2017). No protons are involved in the electro-oxidation of NVP at pH 6-10, while two protons are involved at pH > 10. Therefore, the proposed mechanism is depicted in Scheme 4.2. The dependency of OPS, OPM, MSS/I_p, and MOM on pH were also investigated (**Figure 4.3** and **Table 4.2**).

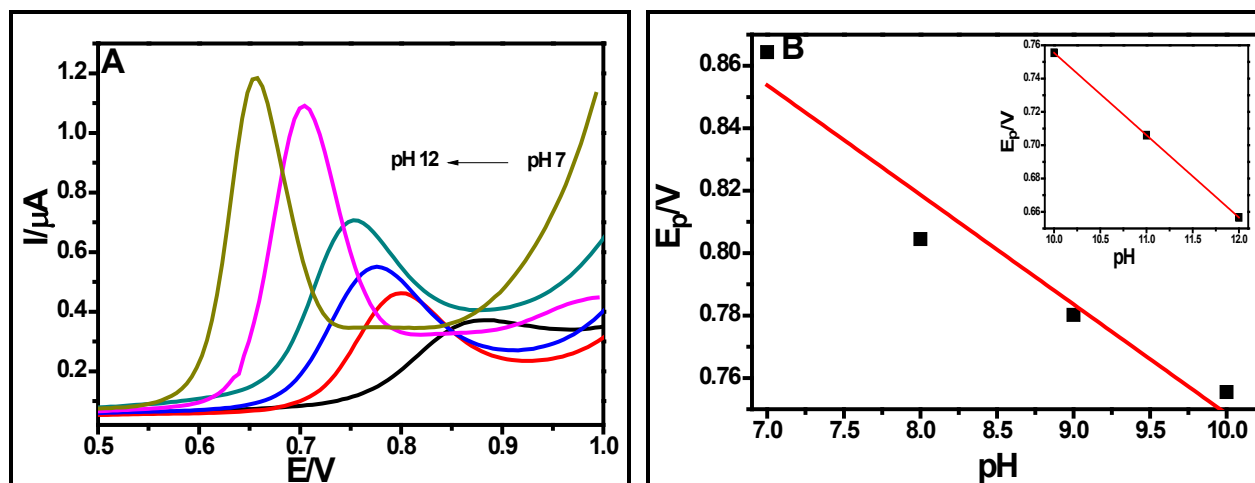
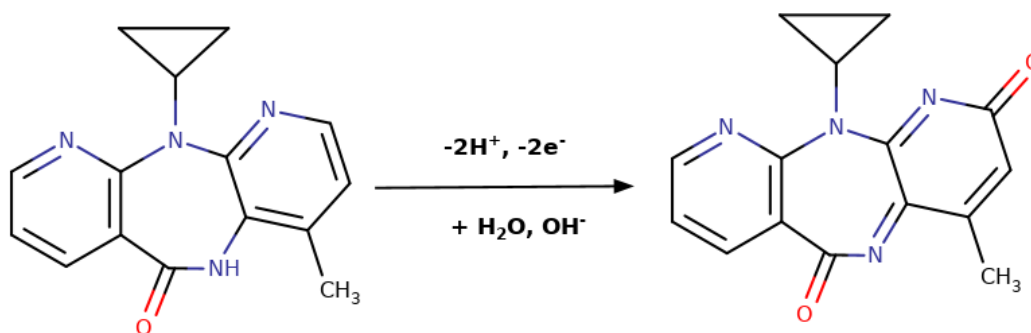


Figure 4.2: SWV of 5 µg.mL⁻¹ NVP at different pHs (7-12) on CPT-BDD reactor (A). Regression plot of E_p vs pH from pH 7-10 and insert: regression plot of E_p vs pH from pH 10-12 (B).

The OPS and OPM of the NVP signal linearly decreased with increasing pH values, while the MSS/I_p linearly increase with pH. The increase in I_p may be due to increased electron-transfer between the positively charged BDD reactor (cathodic pretreatment) and the negatively charged NVP molecule. More negatively charged NVP can easily adsorb on the electrode surface and increase the sensitivity of the BDD reactor. The MOM had a different trend, where it was decreasing and increasing at pH 9 and 11. This may be due to some experimental errors that would be looked at carefully in the next report.



Scheme 4-2: Proposed mechanism for electrooxidation of NVP in alkaline media at BDD reactor.

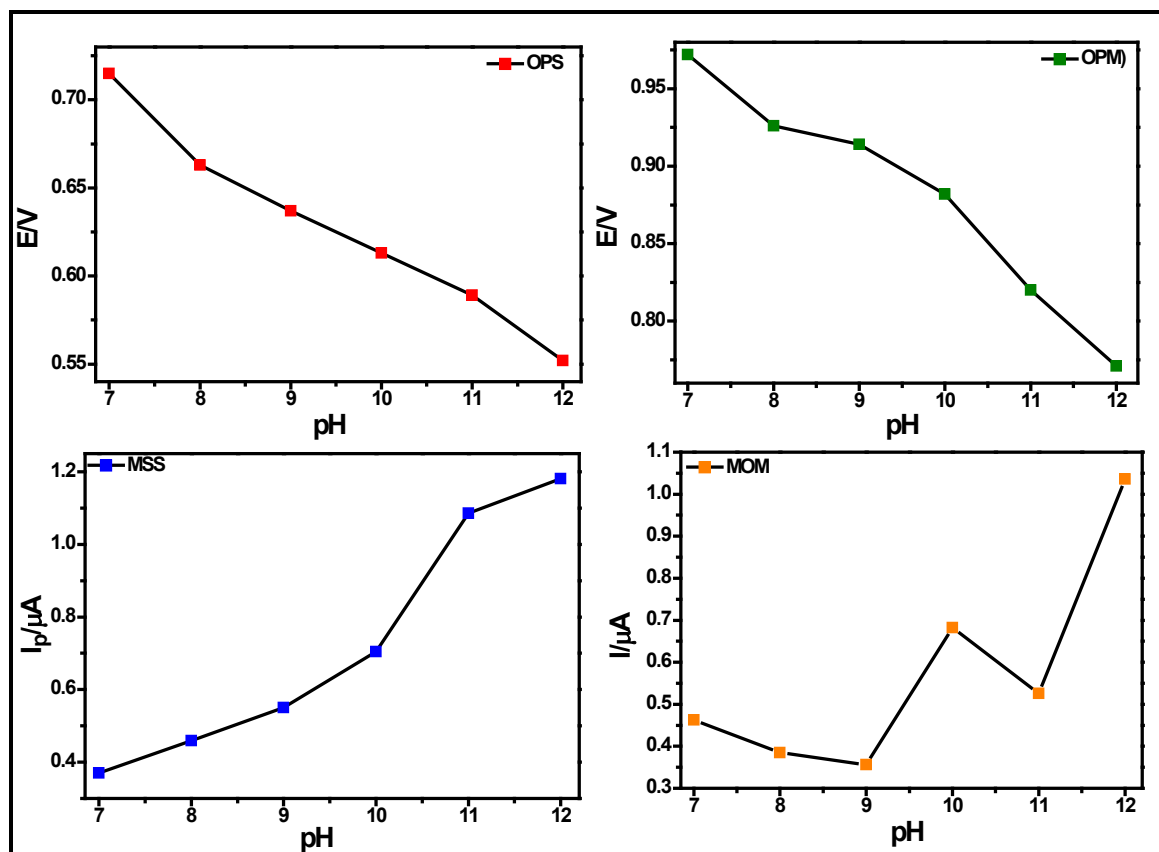


Figure 4.3: pH (pH 7-12) dependence of CPT-BDD reactor parameters for electro-oxidation of 5 µg.mL⁻¹ of the drug in 0.1 M BR [Data plotted were obtained from Figure 4.2.A and Table 4.2.

Table 4.2: Effect of pH on electro-oxidation parameters of 5 µg.mL⁻¹ NVP

pH	OPS (V)	OPM (V)	E _p (V)	MOM (µA)	MSS/I _p (µA)	I _p / [NVP]	RSD (%)
7	0.715	0.972	0.881	0.463	0.370	0.074	3.101
8	0.663	0.926	0.800	0.385	0.459	0.092	3.221
9	0.637	0.914	0.775	0.356	0.550	0.110	2.983
10	0.613	0.882	0.757	0.682	0.704	0.141	3.035
11	0.592	0.820	0.705	0.359	1.086	0.217	2.772
12	0.552	0.771	0.654	1.036	1.181	0.236	2.721

4.2.3 Electroanalytical performance of CPT-BDD reactor containing various concentrations of NVP

After optimization of the BDD reactor's components, quantitative determination of NVP was carried out on the CPT-BDD using differential pulse voltammetry (DPV). This technique was chosen due to its high sensitivity in detecting very low concentrations. **Figure 4.4A** depicts voltammograms of NVP at various concentrations in the BDD reactor. A linear calibration curve was performed in a concentration range of 0.1-50 µg.mL⁻¹ NVP in 0.1 M PB (pH 12) in the BDD reactor. Well-defined oxidation peaks of NVP at different concentrations were observed at 0.68 V, with a slight shift in peak potentials ($\pm 3.5 \times 10^{-3}$ V) after 25 µg.mL⁻¹ concentration. This may be due to insignificant fouling of the electrodes after 6 successive runs without pre-treatment. The calibration curve data obtained from **Figure 4.4B** are presented in **Table 4.3**. The limit of detection (LOD) and limit of quantification (LOQ) were calculated using the formula $b(SD_{bl}/m)$, where b is 3 for LOD and 10 for LOQ, SD_{bl} is the standard deviation of the blank ($n = 6$) at the measured potential and m is the slope of the calibration

curve. The LOD and LOQ were calculated as $0.037 \mu\text{g}\cdot\text{mL}^{-1}$ and $0.12 \mu\text{g}\cdot\text{mL}^{-1}$, respectively. The sensitivity of the sensor was $1.19 \mu\text{A}/\mu\text{g}\cdot\text{L}^{-1}/\text{cm}^2$.

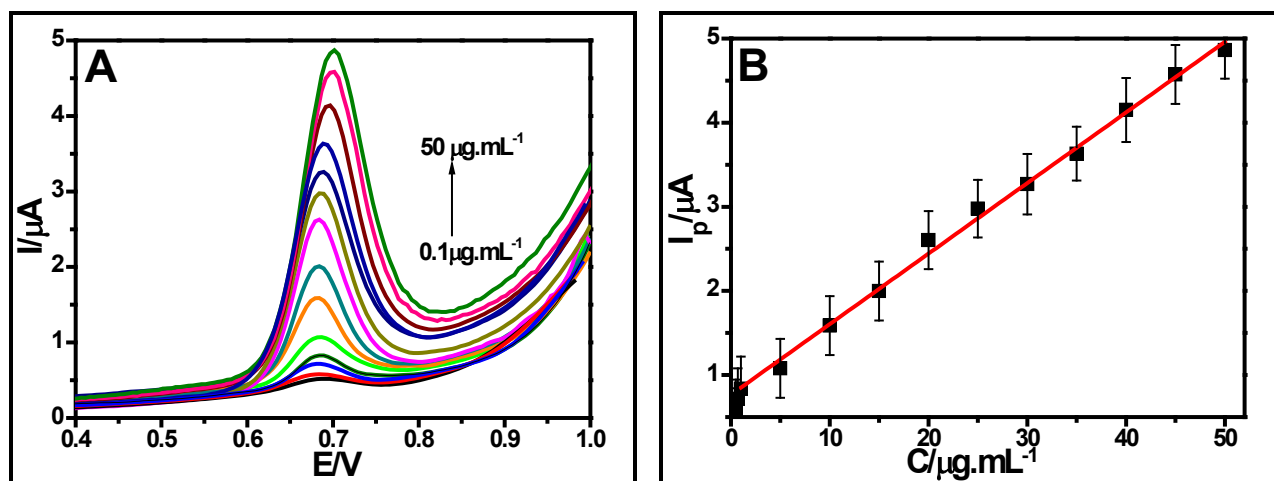


Figure 4.4: DPV response of a CPT-BDD reactor in 0.1 M PB (pH 12) containing various concentrations of NVP ($0.1\text{-}50 \mu\text{g}\cdot\text{mL}^{-1}$) (A). The corresponding calibration curve for the quantification of NVP (B).

Table 4.3: Regression plot data of the calibration curve obtained from square wave voltammetric analysis of NVP at various concentrations in the BDD reactor

Validation parameters	Values
Working concentration range ($\mu\text{g}\cdot\text{mL}^{-1}$)	0.1-50
Linear range ($\mu\text{g}\cdot\text{mL}^{-1}$)	0.1-50
Number of points	14
Slope ($\mu\text{A}/\mu\text{g}\cdot\text{mL}^{-1}$)	0.839
Standard error of the slope	0.00166
y-intercept (μA)	0.756541
Standard error of intercept	0.004915
Standard deviation (SD_{bl}) of blank (μA)	0.0103
Correlation coefficient (R^2)	0.99609
Limit of detection (LOD, $\mu\text{g}\cdot\text{mL}^{-1}$)	0.0368
Limit of quantification (LOQ $\mu\text{g}\cdot\text{mL}^{-1}$)	0.123
Area of the electrode (cm^2)	0.0706
Sensitivity ($\mu\text{A}/\mu\text{g}\cdot\text{mL}^{-1}/\text{cm}^2$)	11.87
RSD (%)	0.358

4.2.4 Application of the proposed method in real water samples

To assess the analytical practicality of the proposed method, DPV and the CPT-BDD electrode were used to detect NVP in wastewater effluent and tap water samples that were spiked with a known concentration of NVP. Without any sample pretreatment, the wastewater sample was spiked with different concentrations of NVP ($0\text{-}25 \mu\text{g}\cdot\text{mL}^{-1}$), and voltammograms were recorded. The analysis of the wastewater effluent without spiking displays no oxidation peak where NVP is oxidised. The absence of NVP oxidation peak at $E_p = 0.68 \pm 0.01 \text{ V}$ means that NVP was undetectable at that level and that no other compound was interfering with its signal. **Figure 4.5A** and **Figure 4.5B** are the calibration curves for NVP analysis in wastewater and tap water, respectively. The calibration curves had the following regression equations:

$$I_p (\mu\text{A}) = 0.0982 C (\mu\text{g.mL}^{-1}) + 0.833 \quad (R^2 = 0.999) \quad (\text{wastewater effluent}) \quad [4.3]$$

$$I_p (\mu\text{A}) = 0.0874 C (\mu\text{g.mL}^{-1}) + 0.748 \quad (R^2 = 0.999) \quad (\text{tap water}) \quad [4.4]$$

Where C is the concentration. The LOD and LOQ for wastewater samples were calculated as 0.09 and 0.274 $\mu\text{g.mL}^{-1}$, respectively. While in the tap water sample LOD and LOQ were 0.038 and 0.114 $\mu\text{g.mL}^{-1}$, respectively.

The recovery data depicted in **Table 4.4** and **Table 4.5** indicates that NVP is present in the wastewater effluent of Zandvliet WWTP, while in the University of the Western Cape tap water it was not detected. The recoveries varied from 96 ± 4.4 to $101 \pm 0.76\%$ in wastewater effluent and 94 ± 3.2 to $99.4 \pm 0.2\%$ in the tap water sample. The high recovery rate may suggest that NVP is present in the water samples or that the developed method was able to recover almost all the NVP that was spiked. Nevertheless, the high recoveries without sample pretreatment confirm that the proposed analytical method can be used for accurate and selective analysis of ARV in complex matrices such as wastewater, biological samples, and pharmaceutical formulations. Since the analyte in the electrolyte is in close proximity to the sensing element (electrode) in solution, almost all the NVP injected may be detected and recovered.

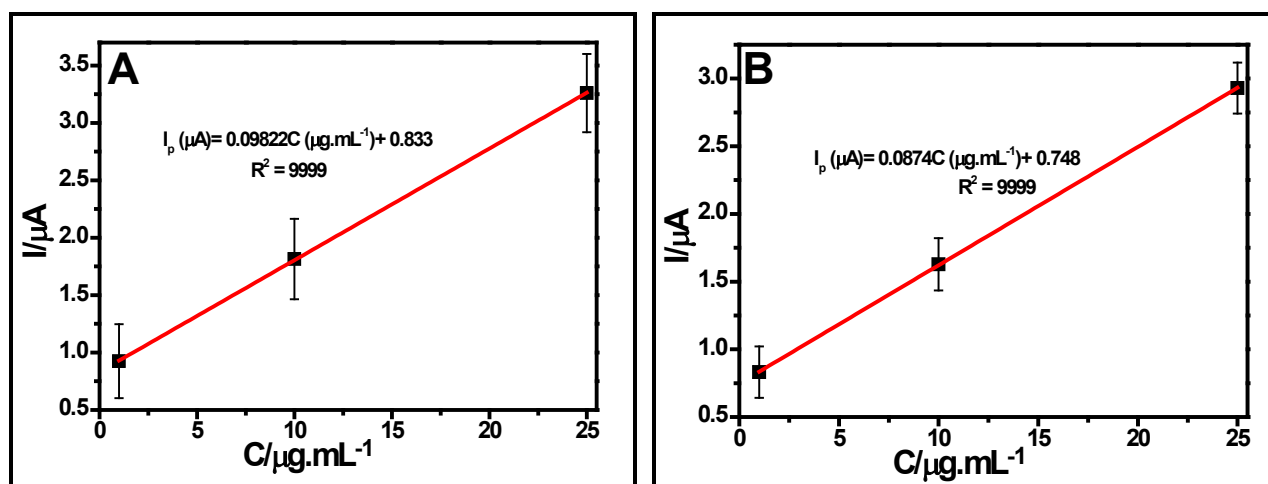


Figure 4.5: Calibration curves for spiked wastewater (A) and tap water (B) samples on a CPT-BDD electrode

Table 4.4: Recovery data of Zandvliet wastewater effluent sample spiked with NVP reference standard. Calibration curve method and DPV were used to obtain the information

Added NVP($\mu\text{g.mL}^{-1}$)	Detected NVP ($\mu\text{g.mL}^{-1}$)	Recovery (%) \pm %RSD (n = 3)
1	0.96	96 ± 4.4
10	10.1	101 ± 0.76
25	24.85	99.4 ± 0.2

Table 4.5: Recovery data of tap water sample spiked with NVP reference standard. Calibration curve method and DPV were used to obtain the information

Added NVP ($\mu\text{g.mL}^{-1}$)	Detected NVP ($\mu\text{g.mL}^{-1}$)	Recovery (%)
1	0.94	94 ± 3.2
10	9.86	98.6 ± 0.5
25	24.87	99.4 ± 0.2

4.3 ELECTROCHEMICAL DYNAMICS OF APT-BDD REACTOR CONTAINING TNF AND QUANTIFICATION OF TNF

4.3.1 Electrochemical behaviour of TNF on BDD reactor

Electrochemical oxidation of TNF on the BDD reactor was studied by CV in BR buffer (0.1 M, pH 4) containing $51.436 \mu\text{g}\cdot\text{mL}^{-1}$ TNF. At a scan rate of $50 \text{ mV}\cdot\text{s}^{-1}$ and a potential range of 0-1.8 V (vs Ag/AgCl), TNF exhibited one well-defined irreversible oxidation peak at 1.42 V (**Figure 4.6**). This was due to the electro-oxidation of the pyrimidine base in the adenine base at acid media. This TNF signal was repeatable at 5 scans (data not shown). The electro-oxidation parameters were also studied and their data is presented in **Table 4.6**. The presence of TNF in the BDD reactor was detected at a potential of 1.31 V (OPS) and it was completely oxidised to 2-oxoadenine base at a potential of 1.42 V (E_p) with an intensity of $2.20 \mu\text{A}$ (MSS). At potentials greater than 1.56 V (OPM), TNF electro-oxidation by-product starts to mineralise into non-toxic components such as water (H_2O) and carbon dioxide (CO_2) and the MOM is at $4.63 \mu\text{A}$. The sensitivity of this electro-oxidation process was $0.44 \mu\text{A}/\mu\text{g}\cdot\text{mL}^{-1}$.

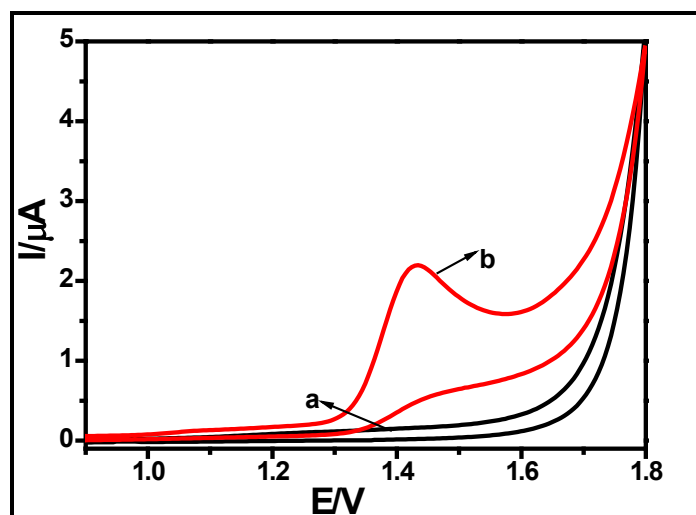


Figure 4.6: Cyclic voltammogram of BDD reactor in the absence (a) and the presence of $1.436 \mu\text{g}\cdot\text{mL}^{-1}$ (b) TNF in 0.1 M Britton Robinson buffer (BR, pH 4) at a scan rate of $50 \text{ mV}\cdot\text{s}^{-1}$.

Table 4.6: BDD reactor's electro-oxidation parameters for 1.436 $\mu\text{g.mL}^{-1}$ TNF [Data obtained from Figure 4.6:]

Parameters	values
Onset potential for sensing (OPS)	1.31 V
Peak current (magnitude of sensing signal, MSS)	2.20 μA
Peak potential (E_p)	1.42 V
Onset potential for mineralization/Decomposition (OPM)	1.56 V
Magnitude of mineralization (MOM)	4.63 μA
Sensitivity [MSS/[TNF]]	0.44 $\mu\text{A}/\mu\text{g.mL}^{-1}$

4.3.2 Effect of electrolyte pH on BDD reactor containing 1.436 $\mu\text{g.mL}^{-1}$ of TNF drug

The pH dependency on electro-oxidation of 1.436 $\mu\text{g.mL}^{-1}$ of TNF through BDD reactor was investigated using square wave voltammetry (SWV) at pH values ranging from 2-8 of 0.1 M BR electrolyte. In the studied pH range, TNF exhibits a single irreversible oxidation peak, however, E_p , MSS/ I_p , OPS, OPM, and MOM are different for each pH value. From pH 2-5, the peak morphology of TNF is well-defined, while that of pH 6-8, the peak is broad. As displayed in **Figure 4.7A**, **Figure 4.8**, and **Table 4.7**, the OPS, OPM, and E_p of TNF linearly shift negatively with increasing pH values of 0.1 M BR, indicating a proton-transfer process. This means that, at acidic media, TNF can be detected and mineralised by just applying lower voltages. MOM and I_p increased with increasing pH until pH 4, then linearly decreased up until pH 8. The decrease in I_p at pH > 4 is due to the absence or poor presence of protons in the electrolyte. The linear relationship between the E_p and the pH resulted in two calibration curves (**Figure 4.7B** and insert) with the following two regression equation:

$$E_{pa} \text{ (V)} = -0.0561 \text{ pH} + 1.60787 \text{ (R}^2 = 0.99979) \text{ (pH 2-4)} \quad [4.5]$$

$$E_{pa} \text{ (V)} = -0.02064 \text{ pH} + 1.45434 \text{ (R}^2 = 0.9548) \text{ (pH 4-8)} \quad [4.6]$$

The slope of $-0.0561 \text{ V.pH}^{-1}$ (Equation 4.5), which is close to the Nernstian value of -0.059 V.pH^{-1} , implies that at pH 2-4, equal numbers of protons (H^+) and electrons (e^-) were involved in the electro-oxidation of TNF at the BDD reactor. While the slope value of -0.02064 (Equation 4.6) implies that an unequal number of protons and electrons were involved in the electro-oxidation of TNF at pH > 4 (Morawska, Popławski et al., 2018; Ozcelikay, Dogan-Topal et al., 2018). In addition, the intersection of the two regression lines is at 4.1, which is closer to the reported pKa of 3.75 for TNF (Medscape, 1994-2021; DrugBank, 2005; AusPAR Stribild and Gilead Sciences Inc., 2015). Due to the presence of a similar adenine base group in TNF, adenine (Ade), and adefovir (ADV), Dogan-Topal et al. (Dogan-Topal, Uslu et al., 2009) compared the electrochemical oxidation of TNF to that of Ade and ADV. According to Dogan-Topal, oxidation of TNF at pH 2-4 involves two electrons and two protons transfer, while at pH values higher than 4, the reaction involves two electrons and one proton. The electro-oxidation mechanism of adenine follows a two-step mechanism, where a total loss of $4e^-$ is involved. The first $2e^-$ are lost during the rate-determining step and the last two are lost during electro-oxidation of the electro-active adenine oxidation by-product, 2-oxoadenine to produce 8-oxoadenine (Goncalves, Batchelor-McAuley et al., 2010; Barman and Jasimuddin, 2014; Karimi-Maleh, Bananezhad et al., 2018; Manikandan, Deepa et al., 2020). However, the TNF molecule has phosphonomethoxypropyl group extra than adenine (Morawska, Popławski et al., 2018; Ozcelikay, Dogan-Topal et al., 2018). Therefore, TNF undergoes electro-oxidation that involves only two electrons, instead of 4. The proposed electro-oxidation mechanism of TNF at BDD reactor at pH 2-4 is displayed in **Scheme 4-3**. At pH 4, the peak of TNF was well-defined and had the highest MSS and MOM with excellent repeatability compared to other pH values. Therefore, pH 4 was chosen to perform all related experiments.

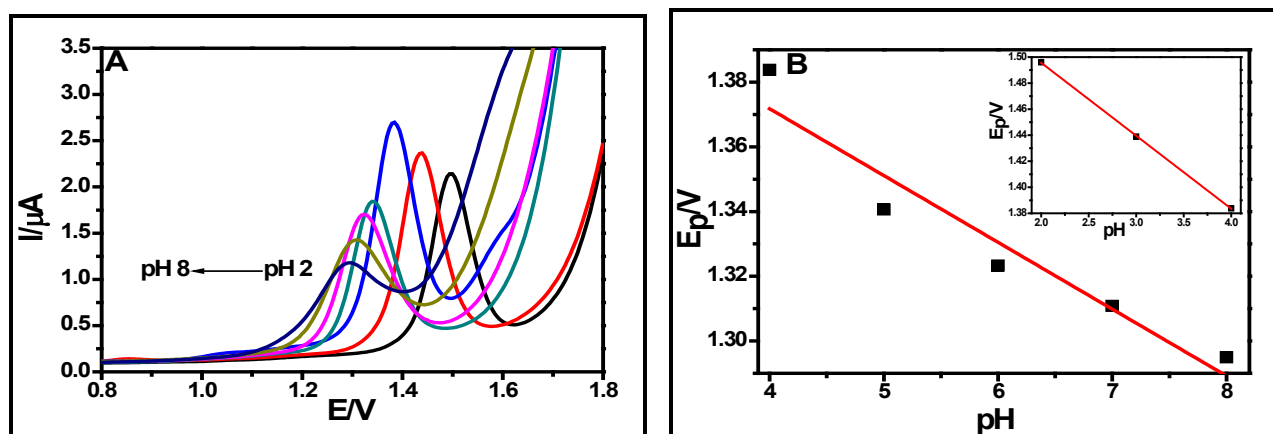


Figure 4.7: Square wave voltammogram of $1.436 \mu\text{g.mL}^{-1}$ TNF at different pH (2-8) on BDD reactor (A). Regression plot E_p vs pH from pH 4-8; insert: Regression plot of E_p vs pH from pH 2-4 (B).

Table 4.7: Effect of pH on electro-oxidation parameters of $1.436 \mu\text{g.mL}^{-1}$ TNF

pH	OPS (V)	OPM (V)	E_p (V)	MOM (μA)	MSS/ I_p (μA)	I_p / [TNF]	RSD (%)
2	1.389	1.629	1.496	2.004	2.140	0.428	2.177
3	1.313	1.573	1.437	2.131	2.368	0.474	3.101
4	1.247	1.499	1.383	7.404	2.798	0.557	2.798
5	1.224	1.489	1.341	7.471	1.839	0.368	3.959
6	1.200	1.472	1.325	6.774	1.703	0.341	2.035
7	1.176	1.443	1.310	5.783	1.425	0.285	2.736
8	1.118	1.411	1.294	5.465	1.171	0.234	3.20

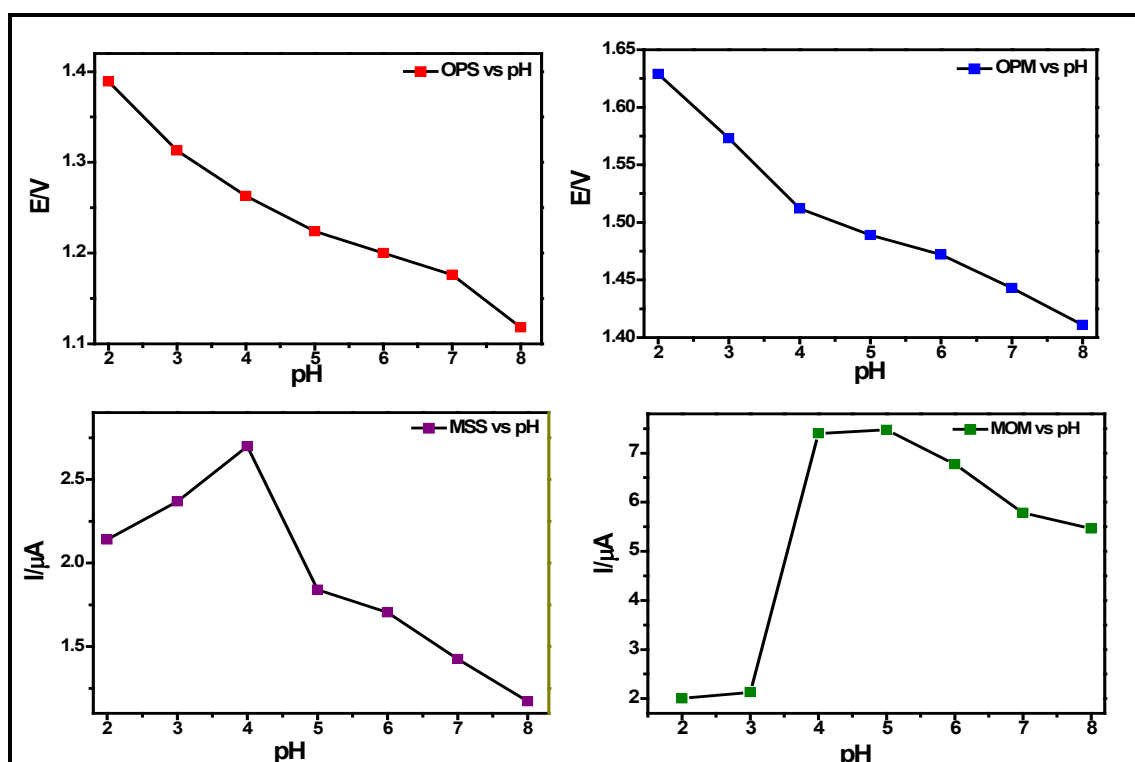
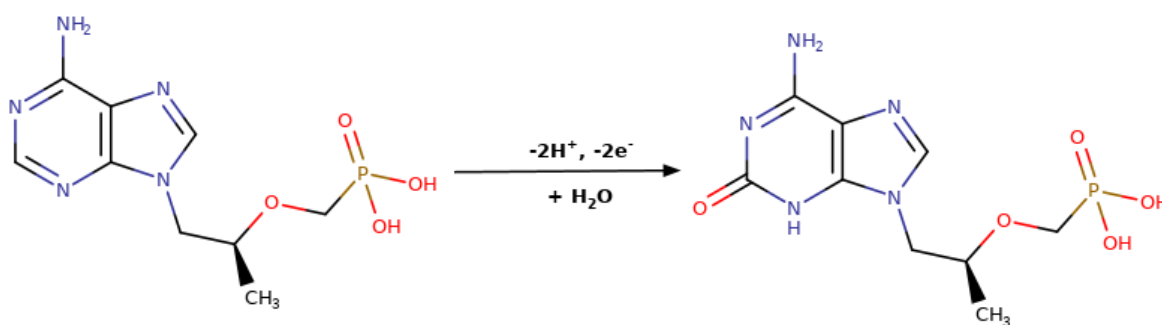


Figure 4.8: pH (pH 2-8) dependence of BDD reactor parameters for electro-oxidation of $1.436 \mu\text{g.mL}^{-1}$ of TNF drug in 0.1 M BR [Data plotted were obtained from Figure 4.7A]



Scheme 4-3: Proposed mechanism of electro-oxidation of TNF in acidic media at the BDD reactor.

4.3.3 Electroanalytical performance of BDD reactor containing various concentrations of TNF

In the chosen electrolyte and pH, TNF exhibited an irreversible anodic peak that increased with increasing concentration over a wide concentration range of 0.014-7.18 $\mu\text{g}\cdot\text{mL}^{-1}$. **Figure 4.9A** displays the DPV of TNF at various concentrations. The inserted graph in **Figure 4.9A** represents the enlarged area where the concentration of TNF is between 0.014 and 1.0 $\mu\text{g}\cdot\text{mL}^{-1}$. The corresponding calibration curve is displayed in **Figure 4.9B**, while its regression parameters are presented in **Table 4.8**. The LOD and LOQ were calculated as 0.00123 and 0.00422 respectively, while sensitivity was $3.565\mu\text{A}/\mu\text{g}\cdot\text{mL}^{-1}/\text{cm}^2$.

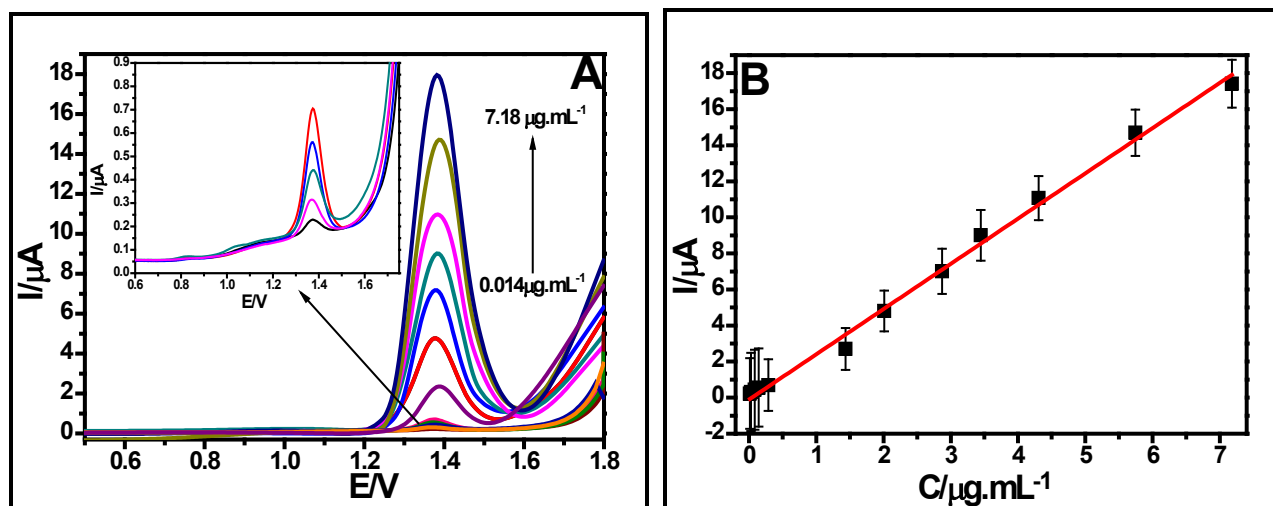


Figure 4.9: SWV of TNF at various concentrations ($0.014\text{-}7.18\mu\text{g}\cdot\text{mL}^{-1}$) in an APT-BDD reactor containing 0.1 BR (pH 4). Insert: Enlargement of DPV at concentration range of $0.05\text{-}1.0\mu\text{g}\cdot\text{mL}^{-1}$.

Table 4.8: Regression plot data of the calibration curve obtained from DPV analysis of TNF at various concentrations in the APT-BDD reactor.

Validation parameters	Values
Working concentration range ($\mu\text{g.mL}^{-1}$)	0.014-7.18
Linear range ($\mu\text{g.mL}^{-1}$)	0.014-7.18
Number of points	12
Slope ($\mu\text{A}/\mu\text{g.mL}^{-1}$)	2.50941
Standard error of the slope	0.0586
y-intercept (μA)	-0.10527
Standard error of intercept	0.21265
Standard deviation of blank (μA)	0.00106
Correlation coefficient (R^2)	0.996
LOD ($\mu\text{g.mL}^{-1}$)	0.00123
LOQ ($\mu\text{g.mL}^{-1}$)	0.00422
Area of the BDD electrode (cm^2)	0.0706
Sensitivity ($\mu\text{A}/\mu\text{g.mL}^{-1}/\text{cm}^2$)	35.565
RSD (%)	1.225

4.3.4 Application of the proposed method in real water samples

To validate the accuracy of the electrochemical method as well as its practicality, recovery experiments on wastewater and tap water spiked with different concentrations of TNF were performed. **Figure 4.10A** and **Figure 4.10B** show the calibration curves for the spiked wastewater effluent and tap water sample, respectively. Wastewater effluent was spiked with 0.029, 0.144, 0.289 $\mu\text{g.mL}^{-1}$, while tap water was spiked with 0.01, 0.05 and 0.1 $\mu\text{g.mL}^{-1}$. The percentage recovery data shown in **Table 4.10** and **Table 4.11** sensor was good as the recovery ranges from 96.6 ± 3.2 to $99.3 \pm 4.0\%$ in wastewater effluent and 95 ± 2.7 to $97.8 \pm 3.1\%$ in the tap water sample. **Table 4.9** shows the regression plot parameters for the standard addition method of TNF in wastewater and tap water. Using the slopes and the standard deviation of the developed method, the LOD, and LOQ in wastewater were determined as 0.0106 and 0.0356 $\mu\text{g.mL}^{-1}$, respectively. While the tap water had a LOD of 0.0159 $\mu\text{g.mL}^{-1}$, the good recovery rate and low LOD and LOQ validate the accuracy and practicality proposed electrochemical method for environmental analysis of TNF.

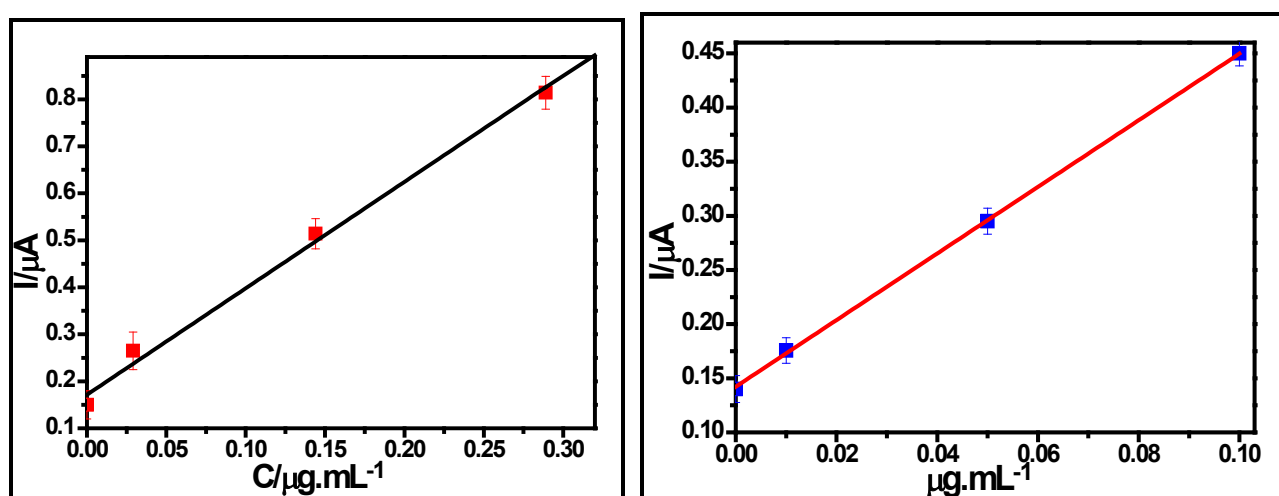


Figure 4.10: Calibration curve of spiked wastewater effluent (A) and tap water (B) samples

Table 4.9: Regression plot data of the calibration curve obtained from square wave voltammetric analysis of TNF at various concentrations in the BDD reactor.

Validation parameters	Wastewater effluent	Tap water
Working concentration range ($\mu\text{g.mL}^{-1}$)	0.029-0.289	0.01-0.1
Linear range ($\mu\text{g.mL}^{-1}$)	0.029-0.289	0.01-0.1
Number of points	3	3
Slope ($\mu\text{A}/\mu\text{g.mL}^{-1}$)	2.265	3.076
Standard error of the slope	0.124	0.0322
y-intercept (μA)	0.171	0.142
Standard error of intercept	0.0197	0.00186
Standard deviation of blank (μA)	0.00182	0.02063
Correlation coefficient (R^2)	0.991	0.999
LOD ($\mu\text{g.mL}^{-1}$)	0.0106	0.0159
LOQ ($\mu\text{g.mL}^{-1}$)	0.0356	0.0561
Sensitivity ($\mu\text{A}/\mu\text{g.mL}^{-1}/\text{cm}^2$)	32.081	43.57
RSD (%)	0.0325	0.03

Table 4.10: Recovery data of Zandvliet wastewater effluent sample spiked with TNF reference standard solution. The calibration curve method and DPV were used to obtain the information

Added TNF ($\mu\text{g.mL}^{-1}$)	Detected TNF ($\mu\text{g.mL}^{-1}$)	Recovery (%) \pm %RSD (n = 3)
0.029	0.028	96.6 \pm 3.2
0.144	0.143	99.3 \pm 2.0
0.289	0.281	97.2 \pm 1.8

Table 4.11: Recovery data of tap water spiked with TNF reference standard solution. The calibration curve method and DPV were used to obtain the information

Added TNF ($\mu\text{g.mL}^{-1}$)	Detected TNF ($\mu\text{g.mL}^{-1}$)	Recovery (%) \pm %RSD (n = 3)
0.01	0.0095	95 \pm 2.7
0.05	0.0489	97.8 \pm 3.1
0.1	0.096	96 \pm 2.2

4.4 ELECTROCHEMICAL DETECTION OF EMTRICITABINE ON A MAGNETIC MOLECULARLY IMPRINTED POLYMER SENSOR

4.4.1 Electrochemical synthesis of magnetic non-imprinted and imprinted polymer sensor

In this study, a molecularly imprinted polymer sensor was developed using para-aminobenzoic acid as the monomer and emtricitabine as the template. During polymerization, it is important to preserve the structure of the template molecule. Hence, preliminary experiments involving the detection of FTC on a bare GCE at PB (pH 2) were carried out in the potential range of -0.3 to 1.3 V; where the monomer (PABA) is electropolymerized, and no redox peaks were observed. The redox behaviour of FTC on bare GCE was also investigated at a wider potential window of 0 to 2.2 V, and an irreversible oxidation peak was observed at 1.65 V (vs Ag/AgCl). As depicted in **Figure 4.11**, the CV of FTC exhibits one irreversible anodic peak at +1.65 V that positively shifts with increasing scan rates. This confirms the irreversible nature of the FTC molecule in acid media. No oxidation or reduction peak was observed between -0.3 V and 1.3 V, meaning FTC is not electroactive in that potential window.

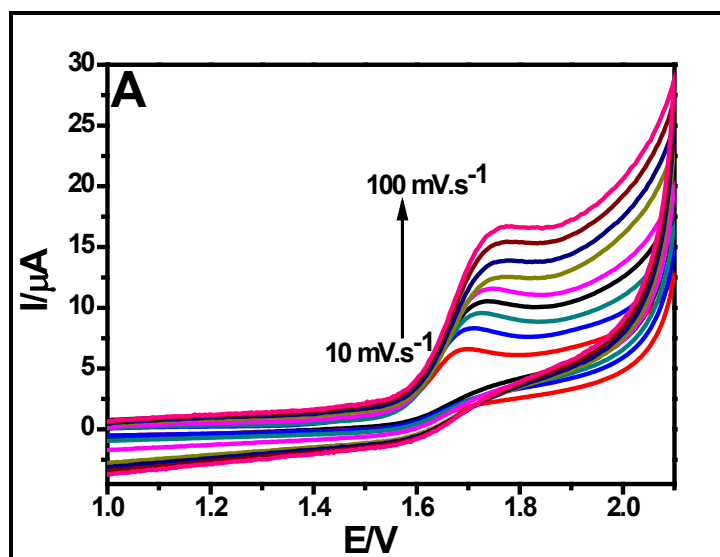


Figure 4.11: Electrochemical behaviour of FTC on a bare GCE at a pH 2 and various scan rates (10-100 V) in the potential range of 0.0 to 2.2 V.

Cyclic voltammetry was employed for the electropolymerization of PABA in the presence (MIP) and absence (NIP) of FTC in 0.1 M H₂SO₄ and potential range -0.3 to 1.3 V at a scan rate of 50 mV.s⁻¹. The continuous electropolymerization of both the NIP and MIP is displayed in **Figure 4.12A** and **Figure 4.12B**, respectively. Firstly, the electrode surface was modified with PABA-modified Fe₃O₄ NPs to increase the conductivity and surface area of the electrode. Moreover, the modified nanoparticles acted as a bridge between the recognition matrix and the electrode surface, thereby enhancing the adsorption and desorption dynamics and kinetics of the template. Secondly, PABA was electropolymerized on the modified electrode in the presence and absence of FTC. According to **Figure 4.11**, electrooxidation of FTC (template) occurs at +1.65 V, which is outside the potential window (0.3-1.3 V) for the electropolymerization of PABA. Therefore, this means that FTC will not be oxidized in that region and will not release electrons to generate current, hence it decreases the peak current of the polymer during polymerization as shown in **Figure 4.12B**. Moreover, there were no new peaks in the presence of FTC, instead, the peaks shifted slightly positive, indicating the blockage caused by FTC during electropolymerization of PABA. During the polymerization of the molecularly imprinted polymer, the template (FTC) molecules are trapped in the polymer matrix because of the molecularly imprinting effect. The nitrogen atoms in the amino group and the ring (-NH₂ and -N-), carbonyl group (C=O), hydroxyl group (-OH) thio group (-S-), ether oxygen (-O-), and the fluorine group (-F-) of the FTC template can form hydrogen bonds with the carboxylic group (-COOH) and the amino group (NH₂) of the p-aminobenzoic acid unit. Furthermore, the presence of the benzene ring in the poly (PABA) may suggest that a recognition site through “π-π stacking” interaction with the aromatic structure of the template may be generated (Liu, Deng et al., 2011; Xiao, Deng et al., 2016). Consequently, the branching and cross-linking of the polymer generate a three-dimensional matrix with cavities containing FTC, and the imprinting process generates a microenvironment for the selective recognition of the FTC molecule based on the shape and complementarity of the functional groups.

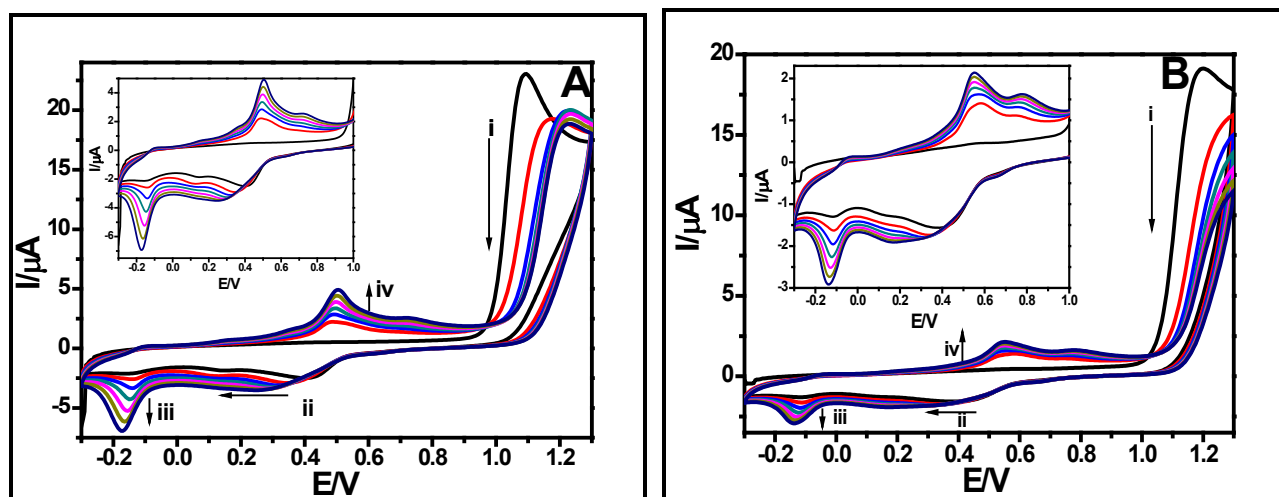


Figure 4.12: Cyclic voltammograms obtained for the electropolymerization of 5.0 mM PABA (A) and PABA-FTC (5:1) (B) in 0.1 M H₂SO₄ on a GCE at a scan rate of 50 mV·s⁻¹ and potential window of -0.3 to 1.3 V using 7 CV scans. The arrows indicate the direction of the current as the number of cycles increases.

4.4.2 Electrochemical characterization of the NIP/PABA-Fe₃O₄/GCE and MIP/PABA-Fe₃O₄/GCE

Cyclic voltammetry (CV), Differential pulse voltammetry (DPV), and electrochemical impedance spectroscopy (EIS) were used to probe the electrochemical properties of the GCE and modified GCE in 0.1 M H₂SO₄. CV and DPV studies were carried out at a scan rate of 50 mV·s⁻¹ in the potential range of -0.3 to 1.3 V. **Figure 4.13A** displays the CV of GCE, Fe₃O₄/GCE, PABA-Fe₃O₄/GCE, NIP/PABA-Fe₃O₄/GCE, and MIP/PABA-Fe₃O₄/GCE. No redox peaks were observed on an unmodified GCE. Upon modification of the GCE with Fe₃O₄, oxidation and reduction peaks appeared at 0.53 and 0.29 V, respectively, indicating the conductivity and electrocatalytic properties of the magnetite nanoparticles. After modification with PABA-capped Fe₃O₄ NPs (PABA-Fe₃O₄), the redox peak currents of Fe₃O₄ NPs increased significantly and the anodic peak slightly shifted to 0.59 V. The cathodic peak broadened and shifted to 0.23 V. Moreover, there are additional broad and low current peaks around 0.98 V and -0.16 V, which indicate that the para-aminobenzoic acid is attached to the magnetites. The broad peak at 0.98 V may be due to the oxidation of the amine group, resulting in a highly reactive amine radical, while the peak at -0.16 V may be due to the progressive reduction of radical. Due to the absence of FTC and high conductivity of poly(PABA) in the NIP/PABA-Fe₃O₄/GCE sensor, the redox current signals of the prepared sensor were further enhanced, and the peak potential shifted slightly negative indicating the electrocatalytic effect of the polymer. However, in the presence of FTC (MIP/PABA-Fe₃O₄/GCE), the anodic and cathodic peak currents decreased significantly and shifted positively, indicating that the non-electroactive (in the applied conditions) FTC that blocks the electron transfer process of the magnetite-polymer modifier was entrapped into the polymer matrix.

EIS is also an efficient tool to study the interfacial properties of the modified electrodes. A typical impedance spectrum consists of a semicircle portion and a linear portion. The semicircle diameter at higher frequencies corresponds to electron/charge-transfer resistance (R_{ct}), while the linear portion at lower frequencies corresponds to diffusion processes (Chen, Zhang et al., 2014). **Figure 4.13B** presents the EIS spectra (Nyquist plots) of GCE as it is modified with different materials and characterized in 0.1 M H₂SO₄ containing 5 mM [Fe(CN)₆]^{3-/4-}, while **Table 4.12** consists of the R_{ct} values and RSD for the different electrode materials. The large R_{ct} value for GCE may be due to the electrostatic repulsion between the negatively charged [Fe(CN)₆]^{3-/4-} redox probe and the negative charge on the carbon of the GCE. In an acidic medium, Fe₃O₄ is positively charged, hence the modification of GCE with Fe₃O₄ NPs reduced the R_{ct} value. Moreover, the presence of the nanoparticles increases the surface-to-volume ratio of the sensing platform, resulting in a faster electron

transfer compared to GCE. When the nanoparticles were modified with the positively charged conductive PABA (PABA-Fe₃O₄/GCE), the R_{ct} value was further reduced. This is because the PABA-Fe₃O₄ nanocomposite was able to attract the negatively charged redox probe to its surface and enhance the electron transfer process. Due to the high conductivity of the polymerized NIP and increased positive charge atoms, the R_{ct} value of the NIP/PABA-Fe₃O₄/GCE was significantly decreased. This is represented by the very prominent linear portion of This indicates that there is almost no heterogeneous charge-transfer resistance on the electrode surface. However, in the presence of FTC (MIP/PABA-Fe₃O₄/GCE), a larger semicircle emerged. This indicates that the non-electroactive macromolecule (FTC) was occupying the cavities in the polymer, resulting in a kinetic barrier for the charge transfer. However, the resistance was not greatly enhanced as the electrode was still able to attract more [Fe(CN)₆]^{3-/4-} ions to its surface. After template elution (MIP/PABA-Fe₃O₄/GCE (extraction)), the R_{ct} significantly decreased. This is because the cavities on the polymer film were now available for charge transfer. Rebinding of the template (MIP/PABA-Fe₃O₄/GCE (rebinding)) increases the charge transfer resistance confirming that the FTC molecules were selectively binding to the generated cavities. The EIS results are in accordance with those in CV, even though the electrolyte was slightly modified

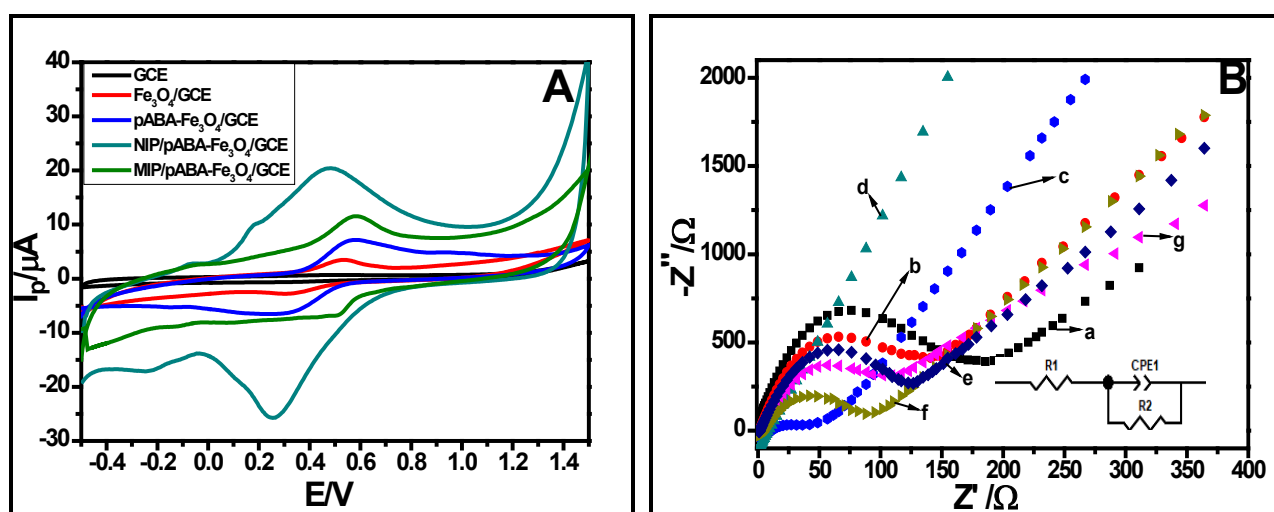


Figure 4.13: Cycle voltammograms of GCE, GCE/Fe₃O₄, PABA-Fe₃O₄/GCE, NIP/ABA-Fe₃O₄/GCE, and MIP/ABA-Fe₃O₄/GCE in 0.1 M H₂SO₄ (A). Nyquist plot spectra of GCE, GCE/Fe₃O₄ (a), PABA-Fe₃O₄/GCE (b), NIP/ABA-Fe₃O₄/GCE (c), MIP/ABA-Fe₃O₄/GCE (d), MIP/ABA-Fe₃O₄/GCE (extraction), (e) and MIP/ABA-Fe₃O₄/GCE (rebinding) (f) in 0.1 M H₂SO₄ containing 1 mM [Fe(CN)₆]^{3-/4-}. Conditions: -0.3 to 1.3 V, scan rate 50 mV.s⁻¹, potential energy 0.5 V, frequencies 10 kHz to 1.0 Hz, amplitude 25 mV

Table 4.12: The charge resistance (R_{ct}) values of the different electrode material employed for sensor fabrication

Electrode material	R _{ct} (Ω)	RSD (%)
GCE	1827.364	1.286
GCE/Fe ₃ O ₄	1351.099	1.333
GCE/Fe ₃ O ₄ -PABA	358.425	1.389
GCE/Fe ₃ O ₄ -PABA/NIP	127.469	1.456
GCE/Fe ₃ O ₄ -PABA/MIP	1264.097	1.441
GCE/Fe ₃ O ₄ -PABA/MIP (extraction)	840.380	1.342
GCE/Fe ₃ O ₄ -PABA/MIP (Rebinding)	1189.997	1.665

4.4.3 Electrochemical detection strategy for the quantification of FTC

The detection strategy for the analysis of FTC was based on observing the electrochemical behaviour of the as-synthesized MMIP rather than that of FTC in 0.1 M H₂SO₄. This is because FTC is irreversibly oxidized at a more positive potential than PABA (≈ 1.7 V and 0.45 V for FTC and PABA, respectively), and higher oxidation potentials are not usually favourable in electrochemistry. Therefore, the MNIP and MMIP were synthesized in the potential range of -0.3 to 1.3 V using 0.1 M H₂SO₄ as an electrolyte. Upon drying, the NIP/PABA-Fe₃O₄/GCE and MIP/PABA-Fe₃O₄/GCE were characterized in 0.1 M H₂SO₄ using CV and SWV in the same potential range. The frequency (f), amplitude (A), and potential steps (E_{step}) were set at 10 Hz, 25 mV, and 5mV, respectively. EIS measurements were also carried out at 0.45 and 0.5 V and frequency range of 1.0 Hz to 10 kHz and amplitude of 5 mV. Therefore every result obtained during optimization studies was referenced to the result of the NIP/PABA-Fe₃O₄/GCE sensor. In this respect, the interaction of the template molecule with the MIP-Fe₃O₄/GCE and NIP-Fe₃O₄/GCE sensors upon its removal from the polymeric film backbone and then rebinding steps were analysed as presented in **Figure 4.14**. The data in **Table 4.13**: were extracted from **Figure 4.14** and depicts the changes in peak current and peak potential values of the sensors in the presence and absence of FTC.

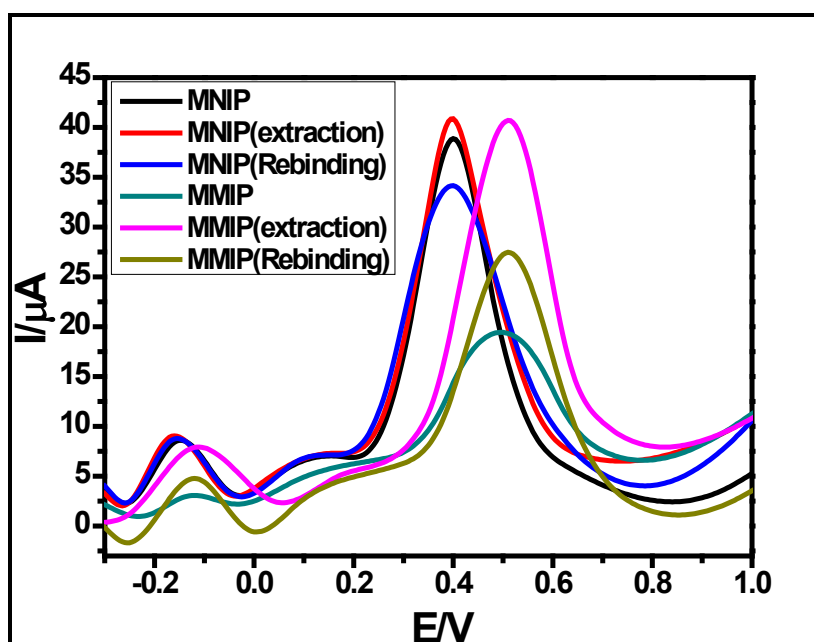


Figure 4.14: SWV voltammetry of Fe₃O₄-NIP/GCE and Fe₃O₄-MIP/GCE in the presence and absence of FTC

Table 4.13: The changes in peak potential (E_p) and peak current (I_p) of the imprinted polymer in the presence and absence of FTC

	I _p before template extraction (μA)	E _p before extraction (V)	I _p after extraction (μA)	E _p after extraction (V)	I _p after template rebind (μA)	E _p after rebinding (V)
Fe ₃ O ₄ -NIP/GCE	37.97	0.42	38.98	0.44	34.53	0.45
RSD (%)	1.497	2.455	2.440	2.256	42393	2.524
Fe ₃ O ₄ -MIP/GCE	17.84	0.53	40.19	0.52	27.64	0.51
RSD (%)	2.324	2.333	2.335	2.665	2.886	2.435

4.4.4 Optimization studies of the parameters that influence the performance of the MMIP sensor

The most important parameters that affect the electrosynthesis and the performance of the MMIP sensor are the monomer and template molar concentration, pH, template extraction and binding time, amount of Fe₃O₄ NPs, and the number of Voltammetric cycles (thickness of the polymer) involved during electropolymerization. Moreover, the extraction solvent has an impact on the developed MNIP and MMIP sensor. Hence, these parameters were evaluated and optimized one variable at a time, and the analysis was carried out in triplicates. Voltammetry was used to monitor the changes in the anodic current (ΔI_p) of the prepared platforms as each parameter was evaluated in 0.1 M H₂SO₄. A pH of 1 (using H₂SO₄), monomer template molar concentration of 5:1, template extraction of 5 min and template rebinding of 3 min, voltammetric scans of 7 (thickness of the polymer), and 0.5 mg.mL⁻¹ of Fe₃O₄ NPs were used for the sensor development.

4.4.5 Analytical performance of Fe₃O₄-MIP/GCE sensor

The analytical performance of the Fe₃O₄-MIP/GCE sensor towards the detection of FTC was carried out using the sensitive DPV technique and the principle of molecular imprinting technology for non-electroactive compounds. The sensitivity of the sensors was increased by the presence of the catalytic Fe₃O₄ NPs and the electrically conducting monomer (PABA) that was employed for the electrosynthesis of the NIP and MIP. Moreover, the MIP increased the selectivity of the sensor by creating recognition cavities where FTC will selectively rebind and conform during detection studies. The change in peak current (ΔI_p) of the sensors as different concentrations of the drug interacts with it was used as the detection/quantification mechanism. After optimization and the extraction of the template from the MMIP, the fabricated Fe₃O₄-MIP/GCE sensor was used for the detection of FTC by immersing the sensor in an electrolyte solution containing different concentrations of FTC for 3 min for the rebinding of the drug on the cavities on the sensor. The current response of the extracted MMIP at 0.51 V gradually decreases with the sequential addition of FTC, and the peak potential experiences a positive shift with increasing FTC concentration. Before the addition of the analyte, the DPV measurements of the sensor was performed in an electrolyte 6 times and the data was recorded as blank and used to calculate the standard deviation (σ) used in calculating the LOD and limit of LOQ.

The DPV curves displayed in **Figure 4.15A** demonstrate the relationship between the concentration of the analyte and the current of the Fe₃O₄-MIP/GCE sensors during electroanalysis. As shown in the graphs by the arrows, the peak currents of a MIP/PABA-Fe₃O₄/GCE sensor decrease with the increasing concentration of the analyte. This is due to the that, the non-electroactive FTC was partially occupying and binding to the electroactive molecularly imprinted cavities through the strong hydrogen bonding and the π - π stacking interactions causing slow electron transfer or blockage at the electroactive magnetic polymer sensor. Hence, the decrease in the peak current signal. The detection studies were performed in the concentration range of 0.01 to 100 $\mu\text{g.mL}^{-1}$, and the sensor had two linear dynamic ranges at 0.01 to 10 $\mu\text{g.mL}^{-1}$ and 1.0 to 100 $\mu\text{g.mL}^{-1}$. The calibration curves in **Figure 4.15B and C** depict the linear dependency of the changes in peak currents (ΔI_p) of the sensors on the concentrations of FTC from 0.01 to 10 $\mu\text{g.mL}^{-1}$ and 1.0 to 100 $\mu\text{g.mL}^{-1}$, respectively. The error bars represent the three ($n = 3$) independent measurements of similar sensors. The linearity observed at 0.01 to 10 $\mu\text{g.mL}^{-1}$ concentration range had a regression equation of

$$\Delta I_p (\mu\text{A}) = 1.287 C_{\text{FTC}} (\mu\text{g.mL}^{-1}) + 1.512 \quad (R^2 = 0.9959) \quad [4.7]$$

While the linear concentration range of 1.0 to 100 $\mu\text{g.mL}^{-1}$ had a regression equation of

$$\Delta I_p (\mu\text{A}) = 0.105 C_{\text{FTC}} (\mu\text{g.mL}^{-1}) + 14.38 \quad (R^2 = 0.9907) \quad [4.8]$$

The slopes in **Eq. 4.7 and 4.8** together with the standard deviations of the blank ($n=6$) were used to determine the LOD, LOQ, and sensitivity of the sensor. The LOD and LOQ were calculated using the standard IUPAC method, which is based on the standard deviation ($N=3$ for LOD and 10 for LOQ) of the sensor in the absence

of the analyte (FTC) and the slope obtained from the calibration plot during detection. In the linear dynamic range of 0.01 to 10 $\mu\text{g}\cdot\text{mL}^{-1}$, a LOD of 0.006 $\mu\text{g}\cdot\text{mL}^{-1}$ and LOQ of 0.02 $\mu\text{g}\cdot\text{mL}^{-1}$ were obtained, while a LOD of 0.074 $\mu\text{g}\cdot\text{mL}^{-1}$ and LOQ of 0.25 $\mu\text{g}\cdot\text{mL}^{-1}$ were obtained for the second linear dynamic range (1.0 to 100 $\mu\text{g}\cdot\text{mL}^{-1}$). The sensitivity of the sensor was calculated using the slope of the calibration curves and the area of the electrochemically active surface area ($A_{\text{GCE}} = 0.0706 \text{ cm}^2$). The sensitivity at 0.01 to 10 $\mu\text{g}\cdot\text{mL}^{-1}$ was 17.885 $\mu\text{g}\cdot\text{mL}^{-1}/\text{cm}^2$, whereas 1.0 to 100 $\mu\text{g}\cdot\text{mL}^{-1}$ linear range had a sensitivity of 1.487 $\mu\text{g}\cdot\text{mL}^{-1}/\text{cm}^2$.

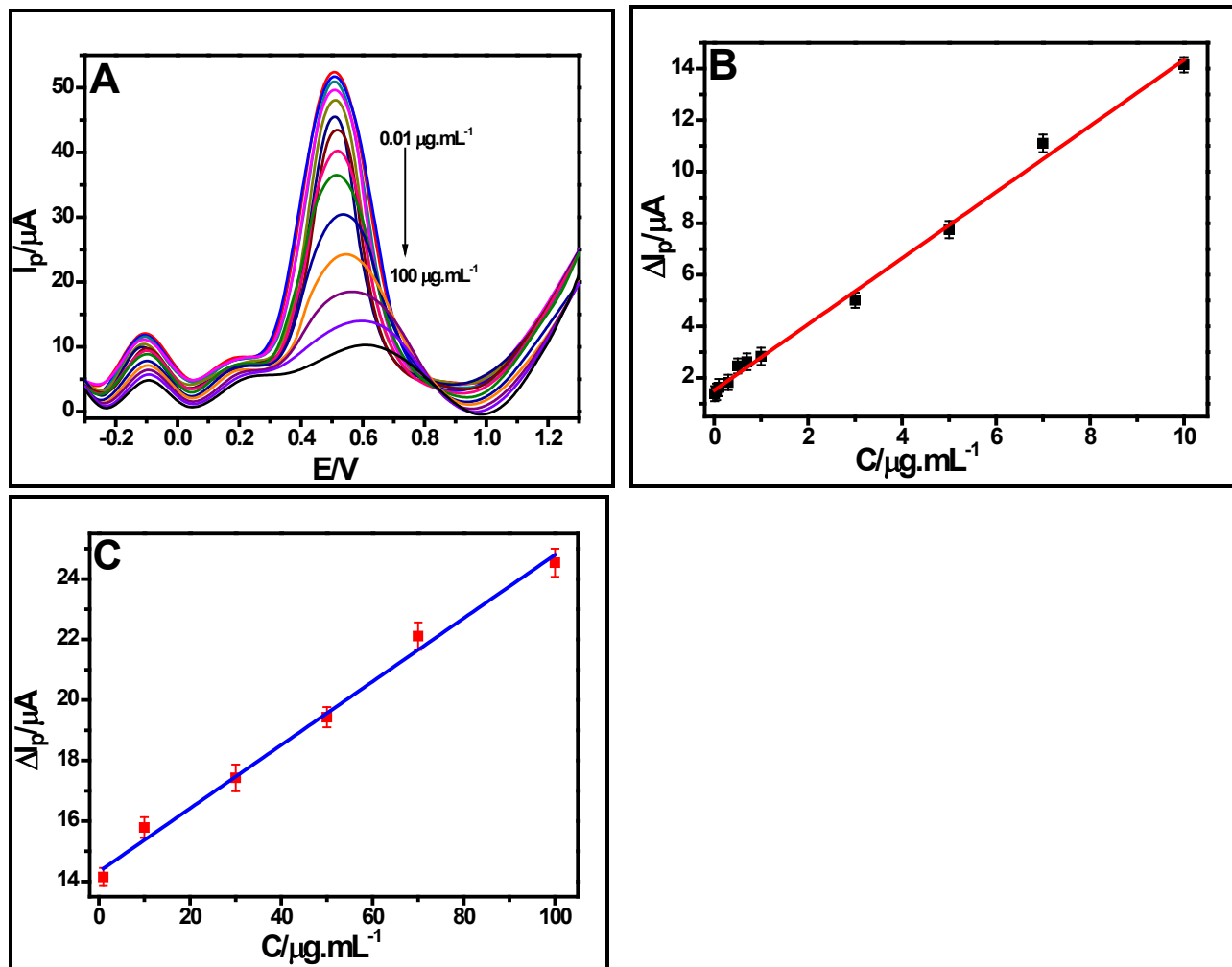


Figure 4.15: DPV plots of MIP/PABA- $\text{Fe}_3\text{O}_4/\text{GCE}$ sensor during rebinding of different concentrations of the FTC template from 0.01 to 100 $\mu\text{g}\cdot\text{mL}^{-1}$ (A). Linear calibration curve for MIP/PABA- $\text{Fe}_3\text{O}_4/\text{GCE}$ at concentration range of 0.01 to 10 $\mu\text{g}\cdot\text{mL}^{-1}$ (B) and 1 to 100 $\mu\text{g}\cdot\text{mL}^{-1}$ (C).

4.4.6 Interference, stability, repeatability, and reproducibility studies

The developed MIP/PABA- $\text{Fe}_3\text{O}_4/\text{GCE}$ and NIP/PABA- $\text{Fe}_3\text{O}_4/\text{GCE}$ sensors were tested in the presence of other species that might be in the environment sample matrix and interfere with its response. The sensors' selectivity was tested in the presence of lamivudine (3TC), efavirenz (EFV), tenofovir (TNF), and nevirapine (NVP). The interfering ARV were chosen because they are usually prescribed together with FTC for the treatment of HIV. **Figure 4.16A** displays a bar graph representing the recorded ΔI_p of the MIP/PABA- $\text{Fe}_3\text{O}_4/\text{GCE}$ sensor in the presence of interfering species, while **Figure 4.16B** represents the ΔI_p recorded for the interferents when using NIP/PABA- $\text{Fe}_3\text{O}_4/\text{GCE}$ sensor. The selectivity coefficient (k) was calculated as ΔI_p (target analyte)/ ΔI_p (interfering species) and the results are presented in **Table 4.14**. Almost no interferences (<10%) were observed in the presence of EFV, TNF, and NVP. This is because these molecules have bigger

molecular sizes than FTC` and their chemical structures are completely different from that of FTC, hence they are restricted from entering and binding into the imprinted cavities on the MIP film. On the other hand, the MMIP sensor greatly responded to 3TC, even though the signal was not that high compared to the FTC signal. The response spring from the fact that the chemical structure of 3TC is almost similar (~90% similarity) to that of FTC and that 3TC has a smaller molecular size than FTC. Therefore 3TC has a chance to manoeuvre to the imprinted sites on the MIP. The only difference between 3TC and FTC is the presence of the fluorine atom in position 5 of the cytidine molecule that makes the MIP sensor to be more sensitive and selective towards FTC than 3TC. In conclusion, the generated recognition cavities on the MIP film were capable of recognizing and distinguishing target molecules through their molecular size, shape, chemical structure, and functional groups distributions. The repeatability of Fe₃O₄-MIP/GCE was examined by measuring the current response of the sensor towards 10 μ M FTC in 0.1 H₂SO₄ for five (5) successive measurements using the same electrode. The cyclic voltammograms in **Figure 4.16C** depict the 5 measurements carried out using the MMIP sensor. The RSD of the five measurements was calculated as 2.67%. This excellent repeatability further proves that the FTC can be extracted and rebonded into the recognition cavities with ease.

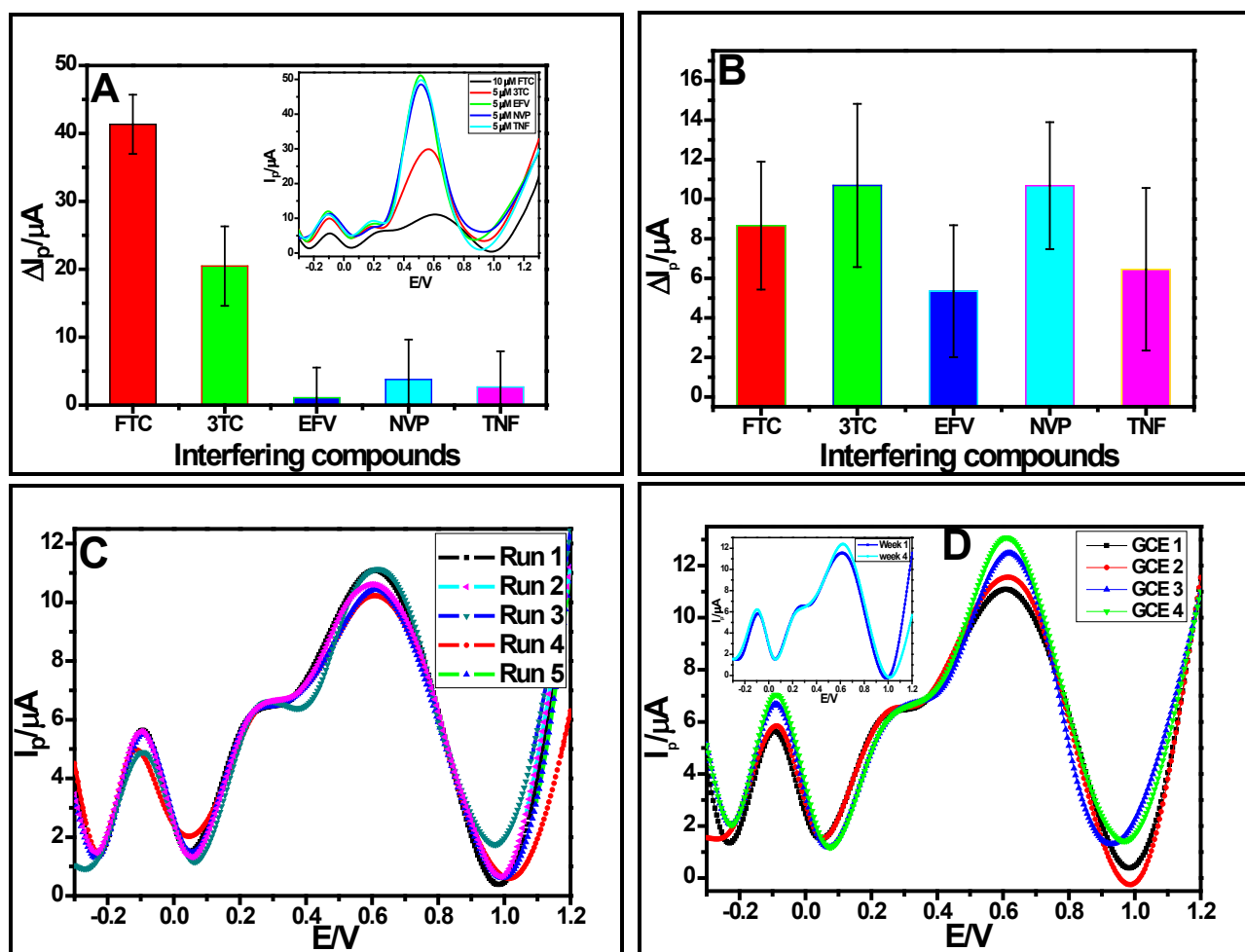
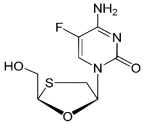
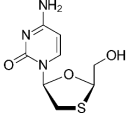
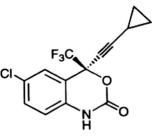
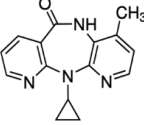
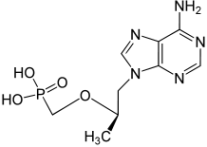


Figure 4.16: Selectivity study of MIP/PABA-Fe₃O₄/GCE (A) and NIP/PABA-Fe₃O₄/GCE (B) in the presence of interfering species such as FTC, 3TC, EFV, TNF, NVP. Repeatability (C), reproducibility (D), and stability (insert D) studies of the MIP/PABA-Fe₃O₄/GCE sensor.

This shows that the MIP/PABA-Fe₃O₄/GCE sensor can be used multiple times with minimum error. For reproducibility studies, four (4) individual MIP/PABA-Fe₃O₄/GCE sensors were fabricated using the same conditions. The sensors were also used for the detection of 10 μ M FTC in 0.1 H₂SO₄ and the voltammograms were recorded as shown in **Figure 4.16D**. The RSD of the sensors during reproducibility tests was 2.25%.

When not in use, the fabricated Fe₃O₄-MIP/GCE was stored at room and its stability over 4 weeks was monitored. The response of the sensor after 4 weeks was 93.8%. The insert in **Figure 4.16D** represents the stability studies.

Table 4.14: Selectivity and relative selectivity data of Fe₃O₄-MIP/GCE and Fe₃O₄-NIP/GCE

Interfering species	Selective coefficient (k _{MMIP})	Selective coefficient (k _{MNIP})	Relative selective coefficient (k' = k _{MMIP} /k _{MNIP})
FTC (MW = 247.25 g.mol ⁻¹) 	1	1	1
3TC (229.26 g.mol ⁻¹) 	2.030	0.808	2.512
EFV (315.66 g.mol ⁻¹) 	38.527	1.621	23.767
NVP (MW=266.30 g.mol ⁻¹) 	11.123	0.805	13.817
TNF (287.21 g.mol ⁻¹) 	15.620	1.355	11.528

CHAPTER 5: CONCLUSIONS AND RECOMMENDATIONS

This project aimed at collecting literature on the presence of antiretroviral drugs in South African wastewater effluent and also aimed at developing electrochemical methods as alternative analytical methods for qualitative and quantitative analysis of antiretroviral drugs in environmental samples.

Antiretroviral drugs have done tremendous work in combating HIV infections since their inception in the 1980s. They have reduced the AIDS-related mortality rate by 64% since 2004. However, their presence in the environment may cause harm to non-targeted organisms. South Africa is one of the countries with a high consumption rate of antiretroviral drugs due to its high HIV/AIDs prevalence. Therefore, is rational to believe that some of these organic compounds are present in the aquatic environment due to their refractory nature and low water solubility. Nevertheless, it has already been proven by several studies that these compounds are present in the environment. The continuous and unmonitored discharge of ARV and other pharmaceutical micropollutants via malfunctioning and inefficient wastewater treatment plants may lead to environmental pollution and catastrophic effect on the aquatic and terrestrial ecosystem. Although these non-biodegradable and recalcitrant pharmaceuticals and their residues currently exist at trace level, they may bioaccumulate and their environmental concentration may increase over time. Hence, sensitive analytical methods that can monitor and quantify these micropollutants at trace levels in water bodies are required. Liquid chromatography coupled with mass spectroscopy (LC-MS/MS) has been extensively and successfully used in quantifying different pharmaceuticals and their residues in environmental samples. However, as an alternative, electroanalytical methods should also be explored for this application, as there are no studies on their environmental electroanalysis. Electrochemical methods have shown their applicability in monitoring ARV in complex clinical and pharmaceutical formulation samples, hence studying their applicability in environmental samples should be interesting.

The present study has already demonstrated the applicability of electroanalytical methods for the analysis of ARV in wastewater effluent and tap water without the need for sample pretreatment. Although the concentration range, LOD, and LOQ were higher compared to the ones reported when using LC-MS/MS. The technology has the potential of being used in analytical chemistry. To enhance the electrochemical performance of the electrochemical method and sensor, the use of electrocatalytic modifiers such as conductive nanomaterials, polymers, and biomolecules is recommended. This will increase the sensitivity and lower the LOD and LOQ of the analytical method. This study explored more on voltammetric methods for quantification of ARV, so other sensitive electrochemical techniques such as chronoamperometry, chronocoulometry, electrochemiluminescence, and photoelectrochemistry, are recommended for exploration in ARV analysis.

The authors recommend studying the effects of interferents on the developed methods and sensor for NVP and TNF analysis. This will assist in also developing a voltammetric method for simultaneous analysis of these drugs as they are usually prescribed in combination. In addition, the electroanalysis of other ARV in wastewater, surface water, groundwater, and drinking water should be extensively studied as there are no studies on the environmental electroanalysis of ARV. Moreover, the developed magnetic molecularly imprinted sensor should be used for selective of FTC in real samples and its recovery studies should be determined. To further improve the application of the analytical method in wastewater, pretreatment of the sample is recommended.

Monitoring the amount of ARV in wastewater effluent is not enough to save our ecosystem, their removal is also very important. Since biodegradation and activated sludge are not active against these micropollutants, we recommend the use of membrane technology and advanced oxidation processes for their complete removal from wastewater.

Due to the lack of analytical facilities, instrumentation, and research funds, South Africa does not have proper and extensive environmental monitoring programs and legislation guidelines for antiviral and other pharmaceutical waste. Currently, there is no information on the maximum permissible concentration of ARV in the environment. Therefore, there is a need for collaborative environmental risk assessment projects between environmental experts in the public and private sectors locally and internationally to come up with the permissible concentration of ARV in the environment.

REFERENCES

- Abafe, O. A., J. Späth, J. Fick, S. Jansson, C. Buckley, A. Stark, B. Pietruschka and B. S. Martincigh (2018). "LC-MS/MS determination of antiretroviral drugs in influents and effluents from wastewater treatment plants in KwaZulu-Natal, South Africa." *Chemosphere* **200**: 660-670.
- African News Agency and Independent Online (IOL). (2019, 26 February 2022). "R1.7bn upgrade underway at Zandvliet Wastewater Treatment Works in Cape Town." Retrieved 10 January, 2022, from <https://www.iol.co.za/news/south-africa/r17bn-upgrade-underway-at-zandvliet-wastewater-treatment-works-in-cape-town-28818192>.
- Ahmadi, E., M. R. Eyvani, V. Riahifar, H. Momeneh and C. Karami (2019). "Amperometric determination of nevirapine by GCE modified with c-MWCNTs and synthesized 11-mercaptopundecanoyl hydrazinecarbothioamide coated silver nanoparticles." *Microchemical Journal* **146**: 1218-1226.
- AL-Ammari, R. H., A. A. Ganash and M. A. Salam (2019). "Electrochemical molecularly imprinted polymer based on zinc oxide/graphene/poly (o-phenylenediamine) for 4-chlorophenol detection." *Synthetic Metals* **254**: 141-152.
- Al-Rajab, A. J., L. Sabourin, R. Chapman, D. R. Lapen and E. Topp (2010). "Fate of the antiretroviral drug tenofovir in agricultural soil." *Science of the total environment* **408**(22): 5559-5564.
- Aminot, Y., X. Litrico, M. Chambolle, C. Arnaud, P. Pardon and H. Budzinski (2015). "Development and application of a multi-residue method for the determination of 53 pharmaceuticals in water, sediment, and suspended solids using liquid chromatography-tandem mass spectrometry." *Analytical and Bioanalytical Chemistry* **407**(28): 8585-8604.
- Asturias-Arribas, L., M. R. Delfino, M. A. Alonso-Lomillo, O. Domínguez-Renedo and M. J. Arcos-Martínez (2016). "Electrochemical Oxidation of the Antiretroviral Drug Nelfinavir on Modified Screen-printed Electrodes." *Electroanalysis* **28**(9): 2081-2086.
- AusPAR Stribild and Gilead Sciences Inc. (2015). STRIBILD®(tenofovir disoproxil fumarate/emtricitabine/elvitegravir/cobicistat) tablets 1-39.
- Awaleh, M. O. and Y. D. Soubaneh (2014). "Waste water treatment in chemical industries: the concept and current technologies." *Hydrology: Current Research* **5**(1): 1.
- Ayankojo, A. G., J. Reut, V. Ciocan, A. Öpik and V. Syritski (2020). "Molecularly imprinted polymer-based sensor for electrochemical detection of erythromycin." *Talanta* **209**: 120502.
- Barletta, J. M., D. C. Edelman and N. T. Constantine (2004). "Lowering the detection limits of HIV-1 viral load using real-time immuno-PCR for HIV-1 p24 antigen." *American Journal of Clinical Pathology* **122**(1): 20-27.
- Barman, K. and S. Jasimuddin (2014). "Electrochemical detection of adenine and guanine using a self-assembled copper (II)-thiophenyl-azo-imidazole complex monolayer modified gold electrode." *RSC Advances* **4**(91): 49819-49826.
- Boulard, L., G. Dierkes and T. Ternes (2018). "Utilization of large volume zwitterionic hydrophilic interaction liquid chromatography for the analysis of polar pharmaceuticals in aqueous environmental samples: Benefits and limitations." *Journal of Chromatography A* **1535**: 27-43.
- Checa, A., R. Oliver, S. Hernández-Cassou and J. Saurina (2009). "Determination of HIV drugs in biological matrices: a review." *Analytica Chimica Acta* **647**(1): 1-13.
- chemicalize.org Nevirapine.
- Chen, H., Z. Zhang, R. Cai, W. Rao and F. Long (2014). "Molecularly imprinted electrochemical sensor based on nickel nanoparticles-graphene nanocomposites modified electrode for determination of tetrabromobisphenol A." *Electrochimica Acta* **117**: 385-392.
- Dévier, M.-H., K. Le Menach, L. Viglino, L. Di Gioia, P. Lachassagne and H. Budzinski (2013). "Ultra-trace analysis of hormones, pharmaceutical substances, alkylphenols and phthalates in two French natural mineral waters." *Science of the total environment* **443**: 621-632.

Dogan-Topal, B., B. Uslu and S. A. Ozkan (2009). "Voltammetric studies on the HIV-1 inhibitory drug Efavirenz: The interaction between dsDNA and drug using electrochemical DNA biosensor and adsorptive stripping voltammetric determination on disposable pencil graphite electrode." Biosensors and Bioelectronics **24**(8): 2358-2364.

DrugBank. (2005, 29 November 2020). "The DrugBank database is a unique bioinformatics and cheminformatics resource that combines detailed drug data with comprehensive drug target information: Nevirapine ". Retrieved 29 November, 2021, from <https://go.drugbank.com/drugs/DB00238>.

DrugBank. (2005, 23 November 2020). "The DrugBank database is a unique bioinformatics and cheminformatics resource that combines detailed drug data with comprehensive drug target information:Tenofovir." . Retrieved 23 November, 2021, from <https://go.drugbank.com/drugs/DB00238>.

Eckhardt, B. J. and R. M. Gulick (2017). Drugs for HIV infection. Infectious Diseases, Elsevier: 1293-1308. e1292.

Esam, Z., M. Akhavan, A. Bekhradnia, M. Mohammadi and S. Tourani (2020). "A Novel Magnetic Immobilized Para-Aminobenzoic Acid-Cu (II) Complex: A Green, Efficient and Reusable Catalyst for Aldol Condensation Reactions in Green Media." Catalysis Letters **150**: 3112-3131.

Feier, B., A. Florea, C. Cristea and R. Săndulescu (2018). "Electrochemical detection and removal of pharmaceuticals in waste waters." Current Opinion in Electrochemistry **11**: 1-11.

Feier, B., A. Gui, C. Cristea and R. Săndulescu (2017). "Electrochemical determination of cephalosporins using a bare boron-doped diamond electrode." Analytica chimica acta **976**: 25-34.

Fisher, I. J., P. J. Phillips, K. M. Colella, S. C. Fisher, T. Tagliaferri, W. T. Foreman and E. T. Furlong (2016). "The impact of onsite wastewater disposal systems on groundwater in areas inundated by Hurricane Sandy in New York and New Jersey." Marine pollution bulletin **107**(2): 509-517.

Freer, J. and V. Mudaly (2022). "HIV and covid-19 in South Africa: The two pandemics must be confronted collectively and globally." British Medical Journal **376**: 1-2.

Funke, J., C. Prasse and T. A. Ternes (2016). "Identification of transformation products of antiviral drugs formed during biological wastewater treatment and their occurrence in the urban water cycle." Water research **98**: 75-83.

Furlong, E. T., A. L. Batt, S. T. Glassmeyer, M. C. Noriega, D. W. Kolpin, H. Mash and K. M. Schenck (2017). "Nationwide reconnaissance of contaminants of emerging concern in source and treated drinking waters of the United States: Pharmaceuticals." Science of the Total Environment **579**: 1629-1642.

Gautam, N., Z. Lin, M. G. Banoub, N. A. Smith, A. Maayah, J. McMillan, H. E. Gendelman and Y. Alnouti (2018). "Simultaneous quantification of intracellular lamivudine and abacavir triphosphate metabolites by LC-MS/MS." Journal of pharmaceutical and biomedical analysis **153**: 248-259.

Gholivand, M. B., E. Ahmadi and M. Haseli (2017). "A novel voltammetric sensor for nevirapine, based on modified graphite electrode by MWCNs/poly (methylene blue)/gold nanoparticle." Analytical Biochemistry **527**: 4-12.

Giri, A. K., C. Charan, A. Saha, V. K. Shahi and A. B. Panda (2014). "An amperometric cholesterol biosensor with excellent sensitivity and limit of detection based on an enzyme-immobilized microtubular ZnO@ ZnS heterostructure." Journal of Materials Chemistry A **2**(40): 16997-17004.

Golla, V. M., M. Kurmi, K. Shaik and S. Singh (2016). "Stability behaviour of antiretroviral drugs and their combinations. 4: Characterization of degradation products of tenofovir alafenamide fumarate and comparison of its degradation and stability behaviour with tenofovir disoproxil fumarate." Journal of pharmaceutical and biomedical analysis **131**: 146-155.

Goncalves, L. M., C. Batchelor-McAuley, A. A. Barros and R. G. Compton (2010). "Electrochemical oxidation of adenine: a mixed adsorption and diffusion response on an edge-plane pyrolytic graphite electrode." The Journal of Physical Chemistry C **114**(33): 14213-14219.

Horn, S., T. Vogt, E. Gerber, B. Vogt, H. Bouwman and R. Pieters (2022). "HIV-antiretrovirals in river water from Gauteng, South Africa: Mixed messages of wastewater inflows as source." Science of The Total Environment **806**: 150346.

- K'oreje, K., L. Vergeynst, D. Ombaka, P. De Wispelaere, M. Okoth, H. Van Langenhove and K. Demeestere (2016). "Occurrence patterns of pharmaceutical residues in wastewater, surface water and groundwater of Nairobi and Kisumu city, Kenya." Chemosphere **149**: 238-244.
- K'oreje, K. O., K. Demeestere, P. De Wispelaere, L. Vergeynst, J. Dewulf and H. Van Langenhove (2012). "From multi-residue screening to target analysis of pharmaceuticals in water: development of a new approach based on magnetic sector mass spectrometry and application in the Nairobi River basin, Kenya." Science of the Total Environment **437**: 153-164.
- Karimi-Maleh, H., A. Bananezhad, M. R. Ganjali, P. Norouzi and A. Sadrnia (2018). "Surface amplification of pencil graphite electrode with polypyrrole and reduced graphene oxide for fabrication of a guanine/adenine DNA based electrochemical biosensors for determination of didanosine anticancer drug." Applied Surface Science **441**: 55-60.
- Kokulnathan, T., E. A. Kumar, T.-J. Wang and I.-C. Cheng (2021). "Strontium tungstate-modified disposable strip for electrochemical detection of sulfadiazine in environmental samples." Ecotoxicology and Environmental Safety **208**: 111516.
- Kozakova, Z., I. Kuritka, N. E. Kazantseva, V. Babayan, M. Pastorek, M. Machovsky, P. Bazant and P. Sáha (2015). "The formation mechanism of iron oxide nanoparticles within the microwave-assisted solvothermal synthesis and its correlation with the structural and magnetic properties." Dalton Transactions **44**(48): 21099-21108.
- Kurmi, M., A. Sahu, A. Balhara, I. P. Singh, S. Kulkarni, N. K. Singh, P. Garg and S. Singh (2020). "Stability behaviour of antiretroviral drugs and their combinations. 11: Characterization of interaction products of zidovudine and efavirenz, and evaluation of their anti HIV-1 activity, and physiochemical and ADMET properties." Journal of Pharmaceutical and Biomedical Analysis **178**: 112911.
- Kurmi, M. and S. Singh (2017). "Stability behavior of antiretroviral drugs and their combinations. 7: Comparative degradation pathways of lamivudine and emtricitabine and explanation to their differential degradation behavior by density functional theory." Journal of Pharmaceutical and Biomedical Analysis **142**: 155-161.
- Lahcen, A. A., A. A. Baleb, P. Baker, E. Iwuoha and A. Amine (2017). "Synthesis and electrochemical characterization of nanostructured magnetic molecularly imprinted polymers for 17- β -Estradiol determination." Sensors and Actuators B: Chemical **241**: 698-705.
- Liu, Y. T., J. Deng, X. L. Xiao, L. Ding, Y. L. Yuan, H. Li, X. T. Li, X. N. Yan and L. L. Wang (2011). "Electrochemical sensor based on a poly (para-aminobenzoic acid) film modified glassy carbon electrode for the determination of melamine in milk." Electrochimica Acta **56**(12): 4595-4602.
- Macpherson, J. V. (2015). "A practical guide to using boron doped diamond in electrochemical research." Physical Chemistry Chemical Physics **17**(5): 2935-2949.
- Manikandan, R., P. Deepa and S. S. Narayanan (2020). "Simultaneous electrochemical determination of adenine and guanine using poly 2-naphthol orange film-modified electrode." Ionics **26**(3): 1475-1482.
- Medscape (1994-2021). emtricitabine/tenofovir AF: Pharmacology
- Mirzajani, R. and S. Karimi (2018). "Preparation of γ -Fe₂O₃/hydroxyapatite/Cu (II) magnetic nanocomposite and its application for electrochemical detection of metformin in urine and pharmaceutical samples." Sensors and Actuators B: Chemical **270**: 405-416.
- Mlunguza, N. Y., S. Ncube, P. N. Mahlambi, L. Chimuka and L. M. Madikizela (2020). "Determination of selected antiretroviral drugs in wastewater, surface water and aquatic plants using hollow fibre liquid phase microextraction and liquid chromatography-tandem mass spectrometry." Journal of hazardous materials **382**: 121067.
- Morawska, K., T. Popławski, W. Ciesielski and S. Smarzewska (2018). "Electrochemical and spectroscopic studies of the interaction of antiviral drug Tenofovir with single and double stranded DNA." Bioelectrochemistry **123**: 227-232.
- Mosekiemang, T. T., M. A. Stander and A. de Villiers (2019). "Simultaneous quantification of commonly prescribed antiretroviral drugs and their selected metabolites in aqueous environmental samples by direct injection and solid phase extraction liquid chromatography-tandem mass spectrometry." Chemosphere **220**: 983-992.

- Nagaraj, V. J., M. Jacobs, K. M. Vattipalli, V. P. Annam and S. Prasad (2014). "Nanochannel-based electrochemical sensor for the detection of pharmaceutical contaminants in water." Environmental Science: Processes & Impacts **16**(1): 135-140.
- Nannou, C., A. Ofrydopoulou, E. Evgenidou, D. Heath, E. Heath and D. Lambropoulou (2019). "Antiviral drugs in aquatic environment and wastewater treatment plants: A review on occurrence, fate, removal and ecotoxicity." Science of The Total Environment: 134322.
- Nannou, C. I., C. I. Kosma and T. A. Albanis (2015). "Occurrence of pharmaceuticals in surface waters: analytical method development and environmental risk assessment." International Journal of Environmental Analytical Chemistry **95**(13): 1242-1262.
- Ncube, S., L. M. Madikizela, L. Chimuka and M. M. Nindi (2018). "Environmental fate and ecotoxicological effects of antiretrovirals: A current global status and future perspectives." Water research **145**: 231-247.
- Ngumba, E., A. Gachanja and T. Tuhkanen (2016). "Occurrence of selected antibiotics and antiretroviral drugs in Nairobi River Basin, Kenya." Science of the Total Environment **539**: 206-213.
- Ngumba, E., P. Kosunen, A. Gachanja and T. Tuhkanen (2016). "A multiresidue analytical method for trace level determination of antibiotics and antiretroviral drugs in wastewater and surface water using SPE-LC-MS/MS and matrix-matched standards." Analytical Methods **8**(37): 6720-6729.
- Ozcelikay, G., B. Dogan-Topal and S. A. Ozkan (2018). "An electrochemical sensor based on silver nanoparticles-benzalkonium chloride for the voltammetric determination of antiviral drug tenofovir." Electroanalysis **30**(5): 943-954.
- Panditi, V. R., S. R. Batchu and P. R. Gardinali (2013). "Online solid-phase extraction-liquid chromatography-electrospray-tandem mass spectrometry determination of multiple classes of antibiotics in environmental and treated waters." Analytical and Bioanalytical Chemistry **405**(18): 5953-5964.
- Panhard, X., M. Legrand, A.-M. Taburet, B. Diquet, C. Goujard and F. Mentré (2007). "Population pharmacokinetic analysis of lamivudine, stavudine and zidovudine in controlled HIV-infected patients on HAART." European Journal of Clinical Pharmacology **63**(11): 1019-1029.
- Pinto-Cardoso, S., N. R. Klatt and G. Reyes-Terán (2018). "Impact of antiretroviral drugs on the microbiome: unknown answers to important questions." Current Opinion in HIV and AIDS **13**(1): 53.
- Prasse, C., M. P. Schlüsener, R. Schulz and T. A. Ternes (2010). "Antiviral drugs in wastewater and surface waters: a new pharmaceutical class of environmental relevance?" Environmental science & technology **44**(5): 1728-1735.
- Rathbun, C. R., M. M. Lewis and M. M. Miller. (2019, 18 April 2019). "Antiretroviral therapy for HIV infections." Retrieved 20 May 2020, from <https://emedicine.medscape.com/article/1533218-overview>.
- Rebelo, P., E. Costa-Rama, I. Seguro, J. G. Pacheco, H. P. Nouws, M. N. D. Cordeiro and C. Delerue-Matos (2021). "Molecularly imprinted polymer-based electrochemical sensors for environmental analysis." Biosensors and Bioelectronics **172**: 112719.
- Rebelo, P., J. G. Pacheco, M. N. D. Cordeiro, A. Melo and C. Delerue-Matos (2020). "Azithromycin electrochemical detection using a molecularly imprinted polymer prepared on a disposable screen-printed electrode." Analytical Methods **12**(11): 1486-1494.
- Reis, N. F. A., J. C. de Assis, S. L. Fialho, G. A. Pianetti and C. Fernandes (2016). "Stability-indicating UHPLC method for determination of nevirapine in its bulk form and tablets: identification of impurities and degradation kinetic study." Journal of Pharmaceutical and Biomedical Analysis **126**: 103-108.
- Rimayi, C., D. Odusanya, J. M. Weiss, J. de Boer and L. Chimuka (2018). "Contaminants of emerging concern in the Hartbeespoort Dam catchment and the uMngeni River estuary 2016 pollution incident, South Africa." Science of the Total Environment **627**: 1008-1017.
- Ross, N., N. Hendricks-Leukes, R. F. Ajayi, P. Baker and E. I. Iwuoha (2015). "Conductive composite biosensor system for electrochemical indinavir drug detection." Journal of Chemistry **2015**.
- Rossmann, J., S. Schubert, R. Gurke, R. Oertel and W. Kirch (2014). "Simultaneous determination of most prescribed antibiotics in multiple urban wastewater by SPE-LC-MS/MS." Journal of Chromatography B **969**: 162-170.

- Sanvicens, N., I. Mannelli, J.-P. Salvador, E. Valera and M.-P. Marco (2011). "Biosensors for pharmaceuticals based on novel technology." TrAC Trends in Analytical Chemistry **30**(3): 541-553.
- Schoeman, C., M. Dlamini and O. Okonkwo (2017). "The impact of a wastewater treatment works in Southern Gauteng, South Africa on efavirenz and nevirapine discharges into the aquatic environment." Emerging Contaminants **3**(2): 95-106.
- Schoeman, C., M. Mashiane, M. Dlamini and O. Okonkwo (2015). "Quantification of selected antiretroviral drugs in a wastewater treatment works in South Africa using GC-TOFMS." Journal of Chromatography & Separation Techniques **6**(4): 1.
- Sgobbi, L. F., C. A. Razzino and S. A. Machado (2016). "A disposable electrochemical sensor for simultaneous detection of sulfamethoxazole and trimethoprim antibiotics in urine based on multiwalled nanotubes decorated with Prussian blue nanocubes modified screen-printed electrode." Electrochimica Acta **191**: 1010-1017.
- Sousa, C. P., F. W. Ribeiro, T. M. Oliveira, G. R. Salazar-Banda, P. de Lima-Neto, S. Morais and A. N. Correia (2019). "Electroanalysis of Pharmaceuticals on Boron-Doped Diamond Electrodes: A Review." ChemElectroChem **6**(9): 2350-2378.
- Swanepoel, C., H. Bouwman, R. Peters and C. Bezuidenhout (2014). "Presence, levels and potential implications of HIV antiretrovirals in drinking, treated and natural waters." Water Research Commission Report K 5.
- Swanepoel, C., H. Bouwman, R. Pieters and C. Bezuidenhout (2015). "Presence, concentrations and potential implications of HIV-anti-retrovirals in selected water resources in South Africa." Water Research Commission. WRC Report(2144/1): 14.
- UNAIDS. (2017, 20 July 2017). "'Ending AIDS: Progress towards 90-90-90 targets' [pdf]" Retrieved 22 January 2020, from https://www.unaids.org/en/resources/documents/2017/20170720_Global_AIDS_update_2017.
- UNAIDS. (2017). "Global AIDS monitoring 2017: indicators for monitoring the 2016 United Nations Political Declaration on HIV and AIDS." Retrieved 22 January 2020, from (http://www.unaids.org/sites/default/files/media_asset/2017-Global-AIDS-Monitoring_en.pdf).
- Veseli, A., F. Mullallari, F. Balidemaj, L. Berisha, L. Švorc and T. Arbnesi (2019). "Electrochemical determination of erythromycin in drinking water resources by surface modified screen-printed carbon electrodes." Microchemical Journal **148**: 412-418.
- Wood, T. P., C. S. Duvenage and E. Rohwer (2015). "The occurrence of anti-retroviral compounds used for HIV treatment in South African surface water." Environmental Pollution **199**: 235-243.
- Wooding, M., E. R. Rohwer and Y. Naudé (2017). "Determination of endocrine disrupting chemicals and antiretroviral compounds in surface water: a disposable sorptive sampler with comprehensive gas chromatography-time-of-flight mass spectrometry and large volume injection with ultra-high performance liquid chromatography-tandem mass spectrometry." Journal of Chromatography A **1496**: 122-132.
- World Health Organization. (2018). "Number of deaths due to HIV/AIDS." Retrieved 22 January 2020, from <https://www.who.int/data/gho/data/indicators/indicator-details/GHO/number-of-deaths-due-to-hiv-aids>.
- World Health Organization. (2019, 14 June 2019). "Drinking-water." Retrieved 10 February 2021, from <https://www.who.int/news-room/fact-sheets/detail/drinking-water>.
- Xiao, N., J. Deng, J. Cheng, S. Ju, H. Zhao, J. Xie, D. Qian and J. He (2016). "Carbon paste electrode modified with duplex molecularly imprinted polymer hybrid film for metronidazole detection." Biosensors and Bioelectronics **81**: 54-60.
- Zhou, C., J. Chen, Q. Xie, X. Wei, Y.-n. Zhang and Z. Fu (2015). "Photolysis of three antiviral drugs acyclovir, zidovudine and lamivudine in surface freshwater and seawater." Chemosphere **138**: 792-797.
- Zhou, C., Y. Wang, J. Chen and J. Niu (2019). "Porous Ti/SnO₂-Sb anode as reactive electrochemical membrane for removing trace antiretroviral drug stavudine from wastewater." Environment international **133**: 105157.
- ZUTARI. (2021). "Zandvliet wastewater treatment works (WWTW), Western Cape, South Africa." Retrieved 26 February 2022, from <https://www.zutari.com/project/zandvliet-water-treatment-works/>.